Modeling the Diversity of Outer Planetary Systems

Harold F. Levison
Space Science Department, Southwest Research Institute, Boulder, CO 80302

Jack J. Lissauer
NASA/Ames Research Center, Moffett Field, CA 94035

and

Martin J. Duncan
Department of Physics, Queen's University, Kingston, Ontario, Canada K7L 3N6

ABSTRACT

In order to better understand the range of dynamically long-lived giant-planet systems, we present the results of a set of bottom-up numerical simulations designed to generate plausible giant planet systems from a large number of planetary embryos. Our simulations produced systems that are stable for at least for a billion years and which exhibit a wide range of characteristics. Some of these systems are reminiscent of the outer solar system. The number of planets ranged from one to seven. Many systems contained only Uranus-mass objects. We constructed systems that were more compact than the outer solar system and systems that were much sparser, with planets on very eccentric orbits. Perhaps most surprisingly, some of the systems that we constructed were stable for at least a billion years despite undergoing macroscopic orbital changes on much shorter timescales.

Subject headings: solar system: formation — solar system: general — celestial mechanics, stellar dynamics

1. Introduction

One of the most important astronomical advances in the last decade has been the discovery of planets around other stars. Although such a discovery was expected, the nature of the systems discovered came as a complete surprise. Due to observational selection effects of the radial velocity technique, all the planets thus far found around normal stars

have masses of the order of Jupiter's mass ($M \gtrsim 0.5 M_{Jup}$). However, their orbital characteristics are quite different from what was expected from studying the giant planets in the solar system. Semi-major axes have been found as small as $0.046\,AU$ (τ Boo; Butler et al. 1997) and eccentricities have been found as large as 0.68 (16 CygB; Cochran et al. 1997). (See http://wwwuser.obspm.fr/planets for current data and bibliographies on extra-solar planets.) Moreover, one planet dominates the radial velocity measurements of these stars over the timescales thus far observed by far more than Jupiter dominates the Sun's motion (Lissauer 1998a). Clearly, these systems have undergone a much different dynamical history than has our solar system.

The current hypotheses for the unexpected diversity of these extra-solar planetary orbits typically rely on dynamical processes. For example, theories attempting to explain the Jupiter-mass planets at small semi-major axes, such as the planet around 51 Peg (Mayor & Queloz 1995), have invoked giant planet orbital migration due to dynamical interactions with either the protoplanetary nebular gas (Lin et al. 1996, Ward 1997) or a putative massive planetesimal disk (Murray et al. 1998). Models attempting to explain the unexpectedly large eccentricities of planets such as those around 70 Vir and 16 CygB have invoked gravitational scattering and/or merging among two (Rasio & Ford 1996), three (Weidenschilling & Marzari 1996) or more (Lin & Ida 1997) unstable giant planets. Alternative models for the planet around 16 CygB have cited the tidal influence of a stellar companion on an inclined single-planet system (Holman et al. 1997, Innanen et al. 1997, Mazeh et al. 1997). Thus, the populations and orbital characteristics of most planetary systems may have been established both by dynamical processes active during the late stages of planet formation and a winnowing produced by billions of years of chaotic 'natural selection'.

Indeed, our own planetary system most likely has been shaped by similar processes. Numerical experiments by several groups over the past decade have made it increasingly apparent that most orbits in our solar system exhibit the chaotic behavior found in many nonlinear Hamiltonian systems (see, e.g., reviews by Wisdom 1987, Duncan & Quinn 1993, Laskar 1996, Lissauer 1998b). However, it is a characteristic of many of these orbits that the timescale for this underlying chaos to produce 'macroscopic' manifestations (e.g., orbit crossings, close encounters, ejections etc.) can be millions to billions or more of orbital periods. Numerical integrations of this duration have recently become feasible, and preliminary results suggest that dynamical effects (including instabilities) may have an important influence on the architecture of planetary systems. In our own system, for example, the unstable nature of nearly all test particle orbits between the giant planets (Gladman & Duncan 1990, Holman 1997) suggests that there is very little room in these regions that could be occupied by additional planets that would produce a configuration which would still survive the age of the solar system. Furthermore, Laskar (1994, 1997) has argued that a similar restriction

applies in the inner solar system, in this case based on the extent of the long-term radial excursions of the current terrestrial planets.

Attempts to perform a general survey of the diversity of outer planetary systems have been very limited. Indeed, the only works of which we are aware are based on a numerical algorithm developed in Dole (1970). (Isaacman & Sagan (1977) extended Dole's original survey to a wider range of initial conditions, but used exactly the same computer software.) In Dole's method, planets are constructed through the accretion of dust and gas (if the planet was massive enough) directly from solar nebula and the occasional merger with other planets. The planetary embryos and planets did not interact with each other gravitationally. Thus, the architectures of these systems are unconstrained by dynamics and many may indeed be gravitationally unstable.

In order to further investigate the possible diversity of long-lived planetary systems, in this paper we present the results of a set of numerical simulations designed to generate plausible giant planet systems from a large number of planetary embryos. We have performed the integrations using a new multiple timestep symplectic code capable of accurately handling close encounters and mergers (Duncan et al. 1998). In addition, we have included a crude recipe for gas drag and accretion. As a result of the later, the simulations are not intended to represent an accurate model for planet formation, but are meant to be a tool to investigate the resulting diversity of those giant planet systems which are ultimately stable for at least one billion years.

The layout of the paper is as follows. In the next section we describe the numerical methods adopted. In Section 3, we discuss the onset of instabilities and the dynamical behavior of unstable systems. We present a statistical analysis of the resulting stable systems in Section 4. In Section 5, we describe, in detail, some of the more interesting systems. Finally, Section 6 contains our concluding remarks.

2. Numerical Methods

In this section, we describe the methods used to construct our planetary systems. It is important to note that we are *not* attempting to model planetary formation. Indeed, at present there is no hope of constructing a computationally realistic and tractable bottom-up, end-to-end simulation of solar system formation because the magnitude of the problem is (among other things) beyond present computer technology. Our goal is only to construct a wide range of dynamically plausible synthetic systems of giant planets, both with and without Jupiter-sized planets. We are not attempting to create terrestrial planets in the current set of simulations.

Our procedure for generating these systems has two steps. First, we generate a set of between 100 and 200 planetary embryos using Monte Carlo techniques and based on a physical description of the protoplanetary disk. Second, we numerically integrate the orbits of these embryos under the graviational influence of the Sun and each other and initially under the influence of the solar nebula, allowing the embryos to merge if they closely approach one another and to accrete nebular gas.

We generate our initial set of planetary embryos using the following simplistic scheme, which is based loosely on the hypothesis that planetary embryos accumulate most of the small bodies in their neighborhoods until they became dynamically isolated from nearby bodies on circular orbits (Lissauer 1987). The embryos were placed in an annulus that extends from 4 to 40 AU from a 1 $M_\odot$ star. The total disk mass in solids is assumed is M_d, and the surface mass density of solids is assumed to vary with distance from the star, r, as $\sigma \propto r^{-\beta}$, where M_d and β are adjustable parameters.

The masses and orbital parameters of the embryos are determined sequentially, beginning with the innermost embryo and moving outwards. The mass of the $i^{\rm th}$ embryo is chosen randomly from a Rayleigh distribution with a mean given by (Lissauer 1993)

$$\overline{M} = \frac{(4\pi B r^2 \sigma)^{3/2}}{(3M_\odot)^{1/2}}, \tag{1}$$

with the values of r and σ taken at the inner edge of the embryo's annular feeding zone (which is the inner edge of the disk for the first embryo). The parameter B is defined as the ratio of the half-width of the embryo's feeding zone to the radius of its Hill sphere, $R_H \equiv r(M/3M_\odot)^{1/3}$, and is taken to be constant for any given system. The outer radius of the embryo's feeding zone, which is taken to be the inner edge of the next embryo's feeding zone, is selected so that the total mass in the zone equals that of the embryo. To ensure that the total mass of all of the embryos equals M_d, the mass of the final embryo is adjusted to achieve the prescribed total mass. The initial orbital radius of the embryo, r_i, is chosen to be

halfway between the inner and outer edges of the embryo's feeding zone. The eccentricity of the embryo is chosen from a Rayleigh distribution with $\overline{e} = 2R_H/r$ (Greenzweig & Lissauer 1990) and the inclination is chosen from a similar distribution with $\overline{\sin i} = R_H/r$. The embryo's mean anomaly, periapse, and ascending node are selected randomly. Note that even though r_i is selected in a deterministic manner, a random component is included in the semi-major axis a_i through the random factors in mass, eccentricity, and initial angles.

We constructed three initial particle loads for our simulations. The parameters for these loads are given in Table 1 and the particle distributions are shown in Figure 1. We initially chose a value of 2.0 for β because it gave roughly equal mass embryos throughout the system. However, as discussed in more detail in §3, this load tended to produce planetary systems where the masses of the planets were not a function of semi-major axis. In order to produce systems that look more like ours (i.e., lower mass planets farther out [1]), we then constructed systems with $\beta = 2.5$. The total disk mass of solids, M_d, was chosen to be a few times the total mass of condensibles in our planetary system ($\sim 60 M_\oplus$ according to recent models of the interiors of Jupiter and Saturn; Guillot et al. 1997). Finally, the ratio of the half-width of the feeding zone to the radius of the Hill sphere, B, is $2\sqrt{3}$ for an isolated embryo in a disk. In order to take into account the fact that embryos are competing with one another, B should be smaller than this. We therefore arbitrary chose $B = \sqrt{3}$ and $B = 1$.

The orbits of the embryos are now integrated by using a new, full N-body, symplectic algorithm known as SyMBA (Duncan et al. 1998). This new code has the speed of the sophisticated, highly efficient computer algorithms known as Mixed Variable Symplectic (MVS) methods (Wisdom & Holman 1991), but in addition it can accurately handle close encounters between objects. Our technique is based on an algorithm that is similar to MVS, but it integrates through encounters by employing a variant of the new multiple step-size techniques (Skeel & Biesiadecki 1994). When bodies are well separated, the algorithm has the speed of MVS, but whenever two bodies suffer a mutual encounter, the step-size for the relevant bodies is recursively subdivided to whatever level is required. This new technique is fast and accurate. Thus, we can integrate our systems of planetary embryos for the times approaching the age of the solar system.

Most of each integration was done using a timestep of 0.1 year. Occasionally a planet reached a sufficiently small periastron distance that the timestep had to be reduced to maintain numerical accuracy. This overall timestep reduction was done in discrete steps

[1]Note that in reality, the decrease in mass of the giant planets in our solar system with increasing distance from the Sun may have resulted from longer formation times for embryos far from the Sun (Lissauer 1987, Pollack et al. 1996) rather than such a large value of β. We did not account for differences in embryo formation times in our simulations.

of about a factor of three and started when the periastron distance fell below $1\,AU$. The timestep of the integration remained reduced at its smallest value until the periastron of the planet either moved to significantly larger distances or the planet was removed from the simulation because its periastron distance dropped below $0.05\,AU$. This overall timestep reduction was done at most a few times during a given run — indeed, in most runs it was not required at all.

In the process of integrating the orbits of the embryos, objects are merged together if they approach one another closer than $f\,(R_{H1}+R_{H2})$, where R_{H1} and R_{H2} are the Hill radii for Body 1 and Body 2, respectively and f is an adjustable parameter. Note that R_H is proportional to $M^{1/3}$ and thus f is the ratio of the physical radius of a planet to the radius of the Hill sphere. In addition, since the initial phases of this process are taking place in the presence of nebular gas, the embryos both feel a drag induced by the gas and accrete nebular gas (if they are large enough). Our prescription for adding gas mass to embryo i, which is crudely based on the results of Pollack et al. (1996), is

$$\dot{M}_i = \begin{cases} 0 & \text{if } M_i < 10M_\oplus, \\ (M_i - 10M_\oplus)/t_g & \text{if } 10M_\oplus < M_i < 100M_\oplus, \\ 90M_\oplus/t_g & \text{if } 100M_\oplus < M_i, \end{cases} \tag{2}$$

where t_g is the characteristic time for doubling for gas. This formula holds for $t < t_{neb}$, where t_{neb} is the lifetime of the nebula; for later times, $\dot{M}_i = 0$ for all values of M_i. The parameters t_g and t_{neb} are adjustable.

If the nebular gas is still present (i.e., when $t < t_{neb}$), then a drag is applied in terms of an acceleration in the direction of a vector between the local Keplerian velocity and the velocity of the embryo, $\mathbf{v}_{rel}$. The acceleration on an embryo is $\mathbf{a} = -\kappa\,\mathbf{v}_{rel}\,(M/M_\odot)^{4/3}$, where κ is an adjustable parameter, and the exponent of $4/3$ arises from the fact that the cross-section of the embryo is enhanced by gravitational focusing of the gas particle trajectories. This drag has the effect of decreasing the inclinations and eccentricities of the embryos. In addition, it causes the embryos to spiral in toward the star. In all of our simulations, this migration was very modest and did not play a significant role in the final structure of the systems. (Note that we did not include two potentially important effects – density waves generated by the planets (Lin et al. 1996, Ward 1997) and partial pressure support – both of which could have lead to significantly larger radial drifts.)

Since our model has seven adjustable parameters, we could only sample a few selected regions of parameter space. It is important to keep this in mind when considering the results presented in §4 and §5. Since we have explored parameter space in a somewhat arbitrary manner, it is inappropriate to take certain statistical measures of our synthetic systems (for example, the relative numbers of one type of system with respect to some other type) too

seriously.

The parameters for our 16 runs are given in Table 2. The choices for these parameters were sometimes motivated by observations, sometimes by experimentation, and sometimes were arbitrary within plausible limits. For example, t_{neb} was chosen to be either 10^6 or 10^7 years, which corresponds to observational limits on the lifetimes of circumstellar gas disks (see the review by Beckwith & Sargent 1996). The maximum value of κ was chosen so that the gas would circularize a Jupiter-mass planet without causing large radial migration over a timescale on the order of t_{neb}. Finally, the value of t_{neb}/t_g was usually chosen to be small enough so that very large planets would not form.

The choice of the parameter f, which is the ratio of the physical radius of a planet to the radius of its Hill sphere, merits a separate discussion. Each of the runs in Table 2 were performed twice. In the first, f is set to 0.1 for the entire length of the simulation. This is very large compared to the current values of f for the giant planets in our solar system ($2 \times 10^{-4} \lesssim f \lesssim 1 \times 10^{-3}$). Our motivation for using such a large value is that we are crudely attempting to include dissipative effects that decrease inclinations and eccentricities while not causing radial migration. We show in the results sections of this manuscript that such dissipative effects are required to form system like our own. Moreover, there are known dissipative effects that are not explicitly included in our simulation. In particular, we have neglected the potentially important effects of a large population of low mass planetesimals (see Levison & Stewart 1999). We refer to this set of $f = 0.1$ runs as Series a and individual runs within it as 'Run $\#_a$', where # is the run number.

In the second series of runs, we set $f = 0.1$ for the first 10^7 years on the grounds that the gas giants have large envelopes in this phase of their evolution (Pollack et al 1996). Thereafter we set f to 7×10^{-4}, which is the mean value for the giant planets in our solar system. We refer to this set of runs as Series b and individual runs within it as 'Run $\#_b$'.

We follow each system until it has been stable for at least a billion years. By stable, we mean that the planets have been on non-crossing orbits for that length of time. Note that this implies that the integrations lasted longer than a billion years and in some cases much longer. Indeed, in one case, planets remained on crossing orbits for 12 billion years (!), at which point the calculation was terminated. In all, each series contains 16 runs, which in principle implies that we constructed 32 systems. However in 4 cases, the runs in Series a and b are the same because the system stabilized in less than 10^7 years. Thus, using the methods above, we created 28 different outer planetary systems, all but one of which were stable by our criteria. Each run took between several weeks and several months on a state-of-the-art workstation.

We wish to emphasize again that we are not attempting to model planet formation. Our goal was to develop a reasonable bottom-up procedure for constructing a wide range of dynamically plausible synthetic systems of giant planets. Some of the assumptions and simplifications described above are not precise analogs to what nature does in practice. However, as is described in more detail below, the systems we construct using the above procedures are in many ways similar to the giant planets in the solar system.

3. The Stability of Systems and the Behavior of Unstable Systems

Although the stability of systems of two planets is largely understood (see e.g., Gladman 1993 and reference therein), the stability properties of systems of more than 2 planets are less well understood. Chambers et al. (1996) integrated systems of 3 or more (in most cases equal mass) planets which began on equally (or nearly equally) spaced coplanar circular orbits. They found that for given masses, the time elapsed before the first pair of orbits crossed, t_c, is well approximated by the formula $t_c \propto e^{c\Delta_o}$, where Δ_o signifies the initial separation in in units of the Hill radii of the planets and c is a constant. In an independent investigation, Duncan & Lissauer (1997) integrated systems with initial orbits identical to subsets of the moons of Uranus, but with the masses of the secondaries all multiplied by the same factor, m_f. They found that the crossing time obeyed a relationship of the form $t_c = m_f^{\alpha}$, where α is a constant for a given system, but varied from $\alpha = -3$ to -13 depending on the system. Duncan & Lissauer (1998) discovered that the same type of power-law mass-scaling relation holds for the four Jovian planets of our solar system, provided $m_f > 3$. The scalings found in these investigations are not yet understood theoretically.

In order to undertake a similar stability analysis for our synthetic planetary systems, we follow the arguments of Lissauer (1995), who developed simple stability criteria based on generalizations of the Hill-Jacobi exclusion zone (Gladman 1993) and the resonance overlap criterion of the restricted 3-body problem (Wisdom 1980). As most long-term orbital instabilities are nonlinear effects associated with overlapping resonances, these criteria provide at best rules of thumb for judging stability. Lissauer's formulae depended only on the masses and semi-major axes of the planets, since they were intended to be applied only to systems where the eccentricities were small (our planetary and some satellite systems). However, some of the planets in our synthetic systems (as well as some recently discovered extra-solar planets) have large eccentricities, implying much closer approaches to neighboring planets than for nearly circular orbits. Thus, we have found it more useful to use a generalized form of Lissauer's stability parameter which accounts for the effects of eccentric motion.

Specifically, for each planet in the system we compute:

$$\zeta_i \equiv \sum_{j}^{a_j<a_i} \frac{a_j}{q_i - Q_j} \left(\frac{M_j}{M_\odot}\right)^{\frac{1}{3}} + \sum_{j}^{a_j>a_i} \frac{a_i}{q_j - Q_i} \left(\frac{M_j}{M_\odot}\right)^{\frac{1}{3}}, \tag{3}$$

where q and Q denote pericentric and apocentric distance, respectively. The larger the value of ζ_i, the larger the perturbations on planet i. Note, however, that Mercury, whose orbit appears to be the least stable of the eight major planets in numerical integrations (Laskar 1994) has the smallest values of ζ. This shows that ζ must be viewed as a global parameter for the entire system, rather than a local one for each specific body (Lissauer 1995). One

can view ζ_i as a crude measure of the potential for chaos in the system arising from the sum of the perturbations on planet i. However, even though the forcing is largest on one particular planet, if that planet is relatively very massive, its response may be much less than those of smaller planets in the system. This is because, in part, it takes less angular momentum transfer to excite high eccentricities in low mass planets. Thus, for each system we determine

$$\zeta_{max} \equiv \max(\zeta_1, \zeta_2 ... \zeta_n). \tag{4}$$

It should noted that Equations (3) and (4) can not be applied to planets that cross the orbits of other planets, such as Pluto. Pluto, however, does not play a significant role in the stability of the outer solar system because of its extremely small mass. Thus, Pluto can be ignored for the above calculation. In our simulations we did not find a system similar to Pluto and Neptune — two planets locked in a mean motion resonance and on crossing orbits.

An alternative criterion based on adding up the ζ values for all planets, or even taking the root of the sum of the squares, could well prove more reliable. However, the fact is that the ζ-criterion is only a rule of thumb for stability, not an exact formulation that always works. Thus, we felt that it is not worthwhile to add unnecessary complexity if this leads to only slightly improved behavior.

In order to study the relevance of the ζ-criterion for our artificial systems, we adopt the following procedure. We take as our sample of systems the Series a runs (i.e., those with large f for the entire length of the calculation). We use this subset of systems since, in some sense, such systems are reset after each merger. This is because the planets remain on relatively low eccentricity orbits for all times in systems with large f. Even when such a system becomes unstable, this instability usually involves only two planets which merge. After the merger, the new planet is again usually on a nearly circular orbit, and we can reset our clock to determine the time until the next orbit-crossing instability. In addition, in order to focus purely on gravitational effects, only those systems without gas are included in this analysis (i.e., $t > t_{neb}$).

Figure 2A shows the relationship between ζ_{max} measured immediately after a merger and the time until the next merger occurs, which we refer to as the 'lifetime' of that system. To inter-compare systems, we have expressed the lifetime in units of the orbital period of the planet in each system having the largest initial value of ζ_{max}. Stable systems are shown as lower limits in the figure. As the figure shows, there is generally a fairly good correlation between ζ_{max} and the system lifetime. However, there are four systems that appear to lie outside the general relationship (open diamonds in Figure 2A). To understand these systems, recall that each planet in a system has an associated value of ζ_i and that ζ_{max} is the largest

of these. For each of the four anomalous cases, the planet that is responsible for the large ζ_{max} is the smallest in the system and has a mass which is typically an order of magnitude or more smaller then the next largest planet. In addition, the unstable bodies all had relatively large eccentricities. When these systems go unstable, the small planet is removed, but the orbital configuration of the other planets remain unchanged. Thus, these instabilities are not global instabilities, unlike the others plotted in Figure 2A, and so can be excluded from consideration.

For comparison, we plot in Figure 2B the lifetimes as a function of ζ_{max} for the 3 major studies of systems with 3 or more secondaries described in the first paragraph of this section. It is interesting to note how tight the correlation is despite the fact that the three sets of simulations (the parameters of which are given in the Figure caption) involved secondary to primary mass ratios ranging from 10^{-9} to 10^{-2}. It is equally clear that the correlation in Figure 2B is steeper than that in Figure 2A, which may result from our current simulations typically having more eccentric orbits and a larger range of planetary masses in a given run. Nonetheless, the two panels agree in the sense that no system for which ζ_{max} was $\lesssim 0.2$ was found to be unstable over the timescale of an integration (which in some cases exceeded a billion orbital periods). Furthermore, no system for which ζ_{max} was $\gtrsim 0.65$ was found to be stable for more than $\sim 10^6$ orbital periods of the planet with the largest ζ_{max}.

The relationship shown in Figure 2 has two uses. First, any analytic theory of planetary system stability must explain it. Second, on the more practicle side, the result that $\zeta_{max} \lesssim 0.65$ will provide an important constraint once radial velocity results become sufficiently refined to detect systems with multiple planets. For example, the otherwise unknown inclination of a system's invariable plane to the observers' line-of-sight could be constrained by the fact that a combination of massive planets in a highly inclined system would satisfy the radial velocity data but violate the stability condition.

The unstable runs in Series b could not be included in Figure 2A because, with one exception, once the planets became orbit-crossing, these systems underwent global instabilities that affected all of the other planets in them. In addition, the planets in these systems never settled down into non-crossing orbits again until the final state was reached — a system with a small number of planets on well separated, eccentric orbits. This type of behavior is illustrated in Figure 3, which shows the temporal evolution of Run 12_b: a system that evolved to retain only one planet. The final configuration is shown[2] in Figure 4B. There are

[2]We present in Figure 4 the architectures of a select sample of our stable systems. Figure 4A shows the giants of our own system for reference. We have adopted the scheme devised by Dole (1970), as described in the Figure caption.

several aspects of the evolution that should be noted. At its most violent stage, all of the planets were on crossing orbits and high inclinations were reached. This was typical of these systems. Indeed, inclinations as high as 90° were common, and in many cases planets were scattered onto retrograde orbits. However, these planets never survived to the end of the simulation (see discussion below).

Global instabilities, such as the one described in the last paragraph, spread out the systems. Although our initial loads extended only to $40\,AU$, we created systems in Series b that contain planets with semi-major axes as large as $\sim 450\,AU$. This most distant planet has an eccentricity of 0.52, which puts its periastron distance at $216\,AU$. Typically what happens in these systems is that the planets spread out as they interact. As planets are removed from the simulation, different regions of the system become isolated from one another. As time goes on, only one planet remains in each of these isolated regions. Therefore, the resulting system contains a small number of planets on eccentric orbits. However, these planets are usually well separated from one another. Figure 4C shows an example of such a system, Run 6_b.

Another interesting phenomenon that occurs is that a significant number of planets are removed from the simulations in Series b because their perihelia dropped below $0.05\,AU$. This inner edge was chosen for numerical convenience, but we believe that most would have eventually hit the star, given that the Kozai mechanism (Kozai 1962) generally appears to be the culprit. This effect becomes important if planets are initially scattered to high inclination, moderately eccentric orbits. The Kozai resonance, which exchanges eccentricity with inclination, drives the inclinations down and the eccentricities up, thereby causing these planets to hit the star. This phenomenon is common – over half the unstable systems in Series b lost some of their planets in this manner. Indeed, 2/3 of the mass of one system was scattered into the star!

The collision of a giant planet with its star would be a very energetic event. Such an impact would almost certainly produce a detectable signature if it occurred in a 'nearby' star, but it is unclear whether it could be distinguished from intrinsic stellar variability even if we were fortunate enough to observe it. However, it is possible that a low density giant planet would be partially or totally tidally disrupted on passages close to the star prior to its periastron being lowered enough to allow for a physical impact. Some of the debris from this tidal stripping might form an observable gas/dust disk in orbit about the star.

Once global instabilities set in, it almost always takes at least 10^7 years for the systems to clear themselves out and stabilize. Indeed, this process can take a very long time. About 30% of the systems take longer than 10^8 years and a small fraction longer than 10^9 years. Indeed, one of our systems (Run 2_b) still had planets on crossing orbits up to 12 billion years

[3], at which time when we finally gave up and stopped the simulations (see Figure 4D). The system had 3 planets in it with masses that ranged from 9 to $15 M_\oplus$. Their semi-major axes ranged from 80 to 450 AU and the 2 outermost planetary orbits crossed. The long dynamical lifetime of this system is due in part to the small masses and long orbital periods. However, this result implies that it would not be surprising if we discover long-lived planetary systems around other stars containing some planets on crossing orbits which are not protected by mean motion resonances (as are Pluto and Neptune).

One of the systems in Series b did not undergo a global instability. Figure 5 shows the temporal evolution of this system. At 2×10^8 years, Run 10_b contained 6 planets. Two planets were large, $197 M_\oplus$ and $280 M_\oplus$ and inside of 10 AU. These planets formed early on when the nebular gas was still present. Between 10 and 40 AU were four planets with masses ranging from 3 to $45 M_\oplus$. At about 3×10^8 years the two middle small planets, $M = 20 M_\oplus$ and $10 M_\oplus$, became unstable. They scattered each other into orbits that crossed the orbits of the two massive inner planets. The two inner massive planets threw the two unstable smaller planets out of the system. The resulting system (Figure 4E) is reminiscent of ours, with two massive inner planets and 2 smaller outer ones. The eccentricities of the planets in the final system range from 0.02 to 0.1.

[3]In their current orbit configuration, the two bodies on crossing orbits have a timescale against a significant mutual gravitational scattering event ($\Delta v \approx$ orbital velocity) that we estimate to be greater then 10^{11} years using the Öpik (1951) equations.

4. Statistics of Final Systems

We begin our analysis of the diversity of long-lived synthetic giant planet systems by discussing the distributions of masses and orbital elements of the planets surviving at the end of each of our ensemble of runs. Figure 6A plots the distributions of final mass versus semi-major axis for all the runs, while Figure 6B plots the distributions of eccentricity versus mass. Recall that the ratio of planetary radius to Hill radius was maintained at $f = 0.1$ throughout each run in Series a, whereas f was reduced after 10^7 years in each run of Series b. Consequently, in Figure 6 we use green symbols for planets produced in Series a and blue symbols for those from Series b. For comparison with real systems, we also plot the four giant planets in our solar system as red stars and the planets around 16 CygB ($M \geq 553 M_\oplus$, $a = 1.7\,AU$, and $e = 0.68$), 47 UMa ($M \geq 770 M_\oplus$, $a = 2.1\,AU$, and $e = 0.09$), and 70 Vir ($M \geq 2,180 M_\oplus$, $a = 0.47\,AU$ and $e = 0.4$) as orange stars. Note that the lower mass limits for these planets are plotted in the figure.

The first thing to notice from Figure 6 is that the planets that we created are similar to the ones found in nature. In particular, the real planets (both in our solar system and others) are virtually indistinguishable from our synthetic planets in the diagram. This result validates our choice of parameters in §2.

From Figure 6, we see that the planets surviving in Series b extended to larger semi-major axes and were typically on much more eccentric orbits than those surviving in Series a. This can be attributed to the fact that when the orbits of adjacent protoplanets crossed, in Series a they typically merge into a body on a less eccentric orbit, while in Series b they usually continue to scatter each other and other bodies. Thus, the runs of Series a had a much larger effective dissipation — dissipation which Figure 6 indicates may be necessary to produce low eccentricity planets.

Figure 7 shows a histogram of the number of planets in our stable synthetic systems, which ranges from 1 to 7. The sum of the black and gray is the distribution for a combination of Series a and Series b. The black shows Series a alone. Recall that since we did not cover the parameter space of our initial conditions with a physically meaningful distribution, the shape of the curves should be viewed with suspicion. However, a comparison between the two series *is* appropriate.

The systems of Series a, which effectively had a source of dissipation active through the whole run, tend to have more planets than that of Series b. In addition, systems with the largest number of planets (≥ 5) only result in Series a and consist only of planets with masses comparable to Uranus and Neptune. For example, Figure 4F shows the architecture of Run 14_a, which is the stable system with the largest number (7) of planets. This system

is made of Uranus-like planets with masses between 4 and $26 M_\oplus$. The semi-major axes and eccentricities of the orbits of the planets in Run 14_a range from 4 and 35 AU and 0.027 and 0.059, respectively. The spacing of the planets is roughly a geometric progression with the ratio of the semi-major axes of adjacent planets about 1.4 (it ranges from 1.33 to 1.55).

At the other extreme are systems with a small number of planets. We have described in §3 the temporal evolution of the only system in our study that resulted in a single planet (Run 12_b, cf. Figures 3 and 4B). This planet has a mass of $343 M_\oplus$, a semi-major axis of 17 AU, and an eccentricity of 0.4. Both Series a and b produced systems with two planets, although they were much more frequent in Series b. In all but one case, these systems consisted of planets on widely spaced orbits (the ratio of semi-major axes ranged from 5 to 50). The eccentricity of at least one planet in each system, and usually that of both planets, was greater than 0.25. Figure 4C shows an example of such a system, Run 6_b.

An additional method of studying these systems is to investigate global dynamics parameters. For example, Figure 8 shows how our stable systems are distributed on a plane of ζ_{max} and $(L_{TC} - L_T)/L_{TC}$. The parameter ζ_{max} is defined in Equation (3) and is a measure of the compactness of the system. The parameter $(L_{TC} - L_T)/L_{TC}$ is the 'angular momentum deficit' and is a measure of the average eccentricity of a system, where L_T is the total angular momentum of the system and L_{TC} is the angular momentum that the system would have if all the planets were on circular, coplanar orbits with unchanged masses and semi-major axes. It can be seen from Figure 8 that the runs in Series a tend to be more compact and have lower average eccentricities than those in Series b. There are two types of exceptions to this. The first is 4 systems that stabilized before 10^7 years, in which case the runs in the two series are the same and are typical Series a-type systems. The second exception was the anomalous Series b system described in §2, Run 10_b (Figure 4E). For this system the values of $(L_{TC} - L_T)/L_{TC}$ and ζ_{max} for the massive planets were practically unchanged when the small planets went unstable. Indeed, with those exceptions, the Series b runs lie above the line $(L_{TC} - L_T)/L_{TC} \approx 0.04$ whereas Series a runs lie below.

Given the marginal stability of our own outer system (Quinlan 1992, Duncan & Lissauer 1998), it is somewhat surprising that it is possible to construct stable systems that are significantly more compact than our own. The most extreme example of this is shown in Figure 4G, Run 11_a. Note that in this system there are 3 very massive planets (totaling 8 times the mass of Jupiter) in the region where Jupiter and Saturn reside in our solar system. Part of this stability may be attributable to the presence of mean motion resonances in the system, as we discuss in §5.

The red star in Figure 8 indicates the location of the outer planets of the solar system. The real solar system lies in the general area occupied by some of our synthetic systems.

However, the synthetic systems tend to lie slightly to the upper right of the real solar system. This could be due to the omission in our simulations of a large number of very small planetesimals. Such objects would tend to circularize the orbits of large objects (decreasing $(L_{TC}-L_T)/L_{TC}$) and may cause the outward migration of the outermost planets (decreasing ζ_{max}, see Fernandez & Ip 1983).

In any case, it is clear from Figure 8 that the only synthetic systems that are similar to the real planetary system are those of Series a. We attribute this result to the fact that, in general, when a system becomes unstable there must be a significant source of dissipation to prevent the mean eccentricity and inclination of the system from growing too large (i.e., $(L_{TC}-L_T)/L_{TC} \lesssim \times 10^{-3}$). Based on these results, we tentatively conclude that our solar system had some source of dissipation until it became dynamically stable.

5. A Smorgasboard of Outer Planetary System Structures

A complete description of the stable synthetic systems we created can be found in Table 3 and Appendix A, which includes animations of orbits and other details of the results. The Appendix is available by link from the electronic edition of this issue and from (URL: http://www.boulder.swri.edu/ hal/diversity/appendixA.html). Table 3 lists the time at which the system stabilized (t_s), the final number of planets (N), the mass of the largest planet (M_{max}), the mass for the smallest planet (M_{min}), the total mass in the planets (M_{tot}), and ζ_{max} for each run in both series. In this section we describe some of the interesting and in some cases surprising dynamics found. These include systems with planets in mean motion resonances and systems that are stable for at least 10^9 years despite undergoing large macroscopic variations.

Mean motion resonances do not exist between the major planets in our solar system, although Jupiter and Saturn are very close to the 5:2 mean motion resonance, and Uranus and Neptune are close to the 1:2. Indeed, the marginal stability the outer solar system has been attributed to its nearness to these mean motion resonances (Quinlan 1992). Mean motion resonances are important in the Galilean satellite system (Peale 1976). Io and Europa are in the 1:2 mean motion resonance and Europa and Ganymede are also in a 1:2. These resonances are, in part, responsible for the warm interiors of these satellites.

Six of the 16 systems created in Series a have planets that are involved in mean motion resonances. One system, which is described in more detail below, has two resonances in it. The most common resonance by far is the 1:2, which accounts for 5 of the 7 resonances found. For example, Run 11_a (Figure 4G), which is the most compact system found in our simulations, has a 1:2 mean motion resonance between the two innermost planets. In Figure 9, we plot the critical argument of this resonance, $2\lambda_2 - \lambda_1 - \mu_1$, where λ_1, and λ_2 refer the mean longitude of the inner and outer planets, respectively, and μ_1 refers to the longitude of periastron of the inner orbit. The small libration amplitude implies that this system is very deep in the resonance.

Run 11_a produced the most compact system in our simulations. It is therefore interesting to determine whether the 1:2 resonance is responsible for its stability. As a test, we decreased the semi-major axis of the innermost planet by $0.25\,AU$, in order to move the system out of the mean motion resonance. This changed the ζ_{max} parameter by less than 10%. We then integrated the new system for 1 billion years. The system was stable. Therefore, we conclude that the 1:2 mean motion resonance was not responsible for the stability of the system.

There are also systems that are near, but not quite in the resonance. Run 4_a is an example of such a system (see Figure 4H). The critical argument $2\lambda_2 - \lambda_1 - \mu_2$ is plotted in

Figure 10. Note that the critical argument at times circulates and at times librates. This type of behavior could be interpreted in two ways. It could indicate that of the objects are trapped in the broad, chaotic separatrix, and/or that the separatrix is moving due to the presence of other planets. Thus, the planet pair could sometimes be within the resonance and sometimes outside. In either case, the two planets involved in the (near) resonance are in chaotic orbits, and yet this system is stable for at least a billion years.

We have found other mean motion resonances in our sample. The two inner planets of Run 5_a (see Figure 4I) are involved in the 7:3 mean motion resonance. Figure 11 shows the critical argument $7\lambda_2 - 3\lambda_1 - 2\mu_2 - 2\mu_1$. The libration in this resonance is very smooth and well behaved, with a libration amplitude of $\sim 120°$.

Run 10_a (see Figure 4J) produced a system with five planets and two mean motion resonances. Planets 2 ($M = 196M_\oplus$) and 3 ($M = 44M_\oplus$) sometimes librate about the 5:3 mean motion resonance. Figure 12A shows the critical argument for this resonance. As described above, this behavior indicates either a broad chaotic zone around the separatrix or a migrating separatrix. Planet 3 is also involved with planet 4 ($M = 19M_\oplus$) in the 1:2 mean motion resonance. The critical argument for it is plotted in Figure 12B. Thus, stable systems that contain multiple planets in interacting resonances can exist.

Perhaps the most surprising result from our simulations is that the two systems from series b that have 3 planets, Runs 4_b and 7_b (Figures 4K and 4L, respectively) show significant macroscopic, quasi-periodic changes and yet are stable for a billion years. The most extreme case is Run 7_b, the temporal behavior of which is shown in Figure 13. In Figure 13, each color represents an individual planet. Figure 13A plots the pericentric distances (q, solid curves) and apocentric distance (Q, dotted curves) of each of the three planets in the system as a function of time. Figure 13b shows the inclinations. Although the semi-major axes of the planets remain approximately constant, Figure 13 shows significant evolution of their eccentricities and inclinations. The most extreme is the innermost planet, which has eccentricity that ranges from 0.02 to 0.93 and inclination that ranges from 1° to 47°!

The dynamical evolution of system that resulted from Run 7_b is best described as one of avoidance, with the center and most massive planet (planet 2) playing the critical role. When it is in its least eccentric state ($e = 0.4$), both the inner (planet 1) and outer (planet 3) planets are at their most eccentric. At this point planet 2 is strongly interacting with planet 3, but not with planet 1. Indeed, both planet 2 and planet 3 are precessing very quickly in this state, while planet 1 is precessing very slowly if at all. This state is shown in the left two panels in Figure 14. When the eccentricity of planet 2 is at a maximum ($e = 0.7$), both of the other planets have their smallest eccentricity. At this point planet 1 and 2 are strongly interacting, as seen in the right two panels of Figure 14, and precessing quickly.

This remarkable system repeats these two extreme configurations several times during the integration and it appears to be stable. An animation of this system can be found in Appendix A (URL: http://www.boulder.swri.edu/ hal/diversity/appendixA.html).

6. Conclusions

The dynamical structure of the newly discovered planetary systems was not expected by most astronomers. In order to better understand how such systems formed and what other surprises may be in store, in this paper we presented the results of a set of numerical simulations designed to generate plausible giant planet systems from a large number of planetary embryos.

This is a bottom-up simulation. Our construction algorithm began with over 100 planetesimals located between 4 and 40 AU from a $1 M_{\odot}$ star. We numerically integrated the orbits of these bodies subject to mutual gravitational perturbations and gas drag for $10^6 - 10^7$ years, merging any pair of planetesimals which passed within one-tenth of a Hill Sphere of one another and adding 'gas' to embryos larger than $10 M_{\oplus}$. Use of such large planetesimal radii provided sufficient damping to prevent the system from excessive dynamical heating. Subsequently, systems were evolved without gas drag, either with the inflated radii (Series a) or with more realistic radii (Series b).

Systems took from a few million years to greater then 10 billion years to achieve a state that met our stability criteria (10^9 years without mergers, ejections, or crossing orbits). The global stability of a planetary system seems to be dependent on the compactness of the system, as measured by ζ_{max} (Equations 3 and 4). No system with $\zeta_{max} \lessapprox 0.2$ was found to be unstable over the timescale of an integration (which in some cases exceeded a billion orbital periods). Furthermore, no system for which $\zeta_{max} \gtrsim 0.65$ was found to be stable for more than $\sim 10^6$ orbital period of the planet with the largest ζ_{max}.

Some of the systems produced in Series a closely resemble our Solar System. Most of the runs using realistic physical radii of the planets (Series b) resulted in global instabilities that led to ejections and/or impacts with the star. When they became stable, these systems tended to contain only a few planets, most of which were in highly eccentric and inclined orbits (cf. Figure 4C). Such a large contrast between systems that had a significant source of damping and those that did not leads us to tentatively conclude that our system had some source of dissipation until it became dynamically stable.

Our simulations produced systems with a wide range of characteristics. Some of the most interesting aspects are:

i) The number of planets ranged from one to seven (cf. Figure 7). Series a systems ranged from 2 to 7 planets with a mode at 4 planets. Series b systems ranged from 1 to 4 planets with a mode at 2 planets.

ii) Many systems contained only Uranus-mass objects (see Figures 4D and 4F for exam-

ples). The masses of largest planet in these systems was as small as $20M_{\oplus}$.

iii) Some of the systems that we constructed are more compact than the giant planets in the solar system. The most extreme case was a system with three very massive planets (totaling 8 times the mass of Jupiter) in the region where Jupiter and Saturn reside in our solar system (Figure 4G).

iv) Many of the systems which underwent scatterings after dissipation had been removed ended up with planets on quite eccentric orbits. Although only one simulated system (12_b) was left with only a single planet, several others (e.g., 4_b, 6_b and 7_b) had planets that were so spread out that one planet would dominate the radial velocity variations of its star over times of a few years or less. Thus, these systems may be quite analogous to the planetary systems of 16 Cyg B and 70 Vir.

v) Six of the 16 stable systems created in Series a have planets that are involved in mean motion resonances. The most common resonance by far is the 1:2, which accounts for 5 of the 7 resonances found. Some systems are deep inside the resonance, while other appear to lie on the separatrix. One system, Run 10_a (Figure 4J), has two resonances in it.

vi) The two systems from Series b that have 3 planets, Runs 4_b and 7_b (Figures 4K and 4L, respectively) show significant macroscopic, quasi-periodic orbital variations and yet are stable for at least one billion years.

We thank Glen Stewart, Bill Ward, and Alan Stern for useful conversations. This work was supported by grants from NASA's Exobiology and Origins of Solar Systems Program. The computer algorithm used here, SyMBA, was designed, in part, from internal funding from the Southwest Research Institute. MJD is grateful for the continuing financial support of Canada's Natural Science and Engineering Research Council.

REFERENCES

Beckwith, S.V.W. & Sargent, A.I. 1996. *Nature* **383**, 139.

Butler, R.P., Marcy, G.W., Williams, E., Hauser, H. & Shirts, P. 1997. *Astrophys. J.* **474**, L115.

Chambers, J.E., Wetherill, G.W. & Boss, A. P. 1996. *Icarus* **119**, 261.

Cochran, W.D., Hatzes, A.P., Butler, R.P. & Marcy, G.W. 1997. *Astrophys. J.* **483**, 457.

Dole, S.H. 1970. *Icarus* **13**, 494.

Duncan, M.J. 1997. In 12^{th} *'Kingston Meeting': Computational Astrophysics*, eds. D. Clarke & M. West. ASP Conference Series **123**, 17.

Duncan, M.J., Levison, H.F. & Lee, M.H. 1998. *Astron. J.* submitted.

Duncan, M.J. & Lissauer, J.J. 1997. *Icarus* **125**, 1.

Duncan, M.J. & Lissauer, J.J. 1998. *Icarus*, in press.

Duncan, M.J. & Quinn, T. 1993. *Ann. Rev. Ast. & Ap.* **31**, 265.

Gladman, B. 1993. *Icarus* **106**, 247.

Gladman, B., & Duncan, M. J. 1990. *Astron. J.* **100**, 1680.

Guillot,T., Gautier, D. & Hubbard, W.M. 1997. *Icarus* **130**, 534.

Greenzweig, Y., & Lissauer, J.J. 1990, *Icarus*, **87**, 40.

Holman, M., Touma, J. & Tremaine, S. 1997. *Nature* **386**, 254.

Innanen, K.A., Zheng, J.Q., Mikkola, S. & Valtonen, M.J. 1997. *Astron. J.* **113**, 1915.

Isaacman, R., & Sagan. C. 1977. *Icarus* **31**, 510.

Kozai, Y. 1962. *Astron. J.* **67**, 591.

Laskar, J. 1994. *Ast. & Ap.* **287**, L9.

Laskar, J. 1996. *Cel. Mech. & Dyn. Ast.* **64**, 115.

Laskar, J. 1997. *Ast. & Ap.* **317**, L75.

Levison H.F. & Stewart G. 1999. In preparation.

Lin D.N.C. & Ida, S. 1997. *Astrophys. J.* **477**, 781.

Lin D.N.C., Bodenheimer, P. & Richardson, D.C. 1996. *Nature* **380**, 606.

Lissauer, J.J. 1987. *Icarus*, **69**, 249.

Lissauer, J.J. 1993. *Ann. Rev. Ast. & Astrophys.* **31**, 129.

Lissauer, J.J. 1995. *Icarus* **114**, 217.

Lissauer, J.J. 1998a. In *Solar System Formation and Evolution*, eds. D. Lazzaro et al. (San Francisco: Astronomical Society of the Pacific), submitted.

Lissauer, J.J. 1998b. *Rev. Mod. Phy.* Submitted.

Mayor, M. & Queloz, D. 1995. *Nature*, **378**, 355.

Mazeh, T., Krymolowski, Y. & Rosenfeld, G. 1997. *Astrophys. J.* **477**, L103.

Murray, N., Hansen, B., Holman, M. & Tremaine, S. 1998. *Science* **279**, 29.

Öpik, E.J. 1951. *Proc. Roy. Irish Acad.* **54A**, 165.

Peale, S. 1976. *Ann. Rev. Ast. & Ap.* **14**, 215.

Pollack, J.B., Hubickyj, O., Bodenheimer, P., Lissauer, J.J., Podolak, M. & Greenzweig, Y. 1996. *Icarus* **124**, 62.

Quinlan, G. 1992. In *Chaos, Resonance and Collective Dynamical Phenomena in the Solar System*, ed. S. Ferraz-Mello (Amsterdam: Kluwer), 25.

Rasio, F. A. & Ford, E. B. 1996. *Science* **274** 954.

Skeel, R. D., & Biesiadecki, J.J. 1994. *Ann. Numer. Math.* **1**, 191.

Ward, W.R. 1997. *Astrophys. J.* **482**, L211.

Weidenschilling, S. J. & Marzari, F. 1996. *Nature* **374**, 619.

Wisdom, J. 1980. *Astron. J.* **85**, 1122.

Wisdom, J. 1987. *Icarus* **56**, 51.

Wisdom, J., & Holman, M. 1991. *Astron. J.* **102**, 1528.

This preprint was prepared with the AAS LaTeX macros v4.0.

Fig. 1.— The mass of our initial proto-planetary embryos as a function of their semi-major axes. We created three different loads: A) $M_d = 100M_\oplus$, $\beta = 2$, and $B = \sqrt{3}$. B) $M_d = 100M_\oplus$, $\beta = 2.5$, and $B = \sqrt{3}$. C) $M_d = 200M_\oplus$, $\beta = 2.5$, and $B = 1$.

Fig. 2.— The dynamical lifetimes (in units of the orbital period of the planet with the largest ζ_i) of various orbital configurations as a function of ζ_{max}. **A)** Results from our simulations. Systems that are stable for more than 10^9 years are shown as lower limits. There is one data point off the scale in the diagram which is stable and has $\zeta_{max} = 0.013$. The open circles represent systems where a very small planet is responsible for the large ζ_{max}. When these systems go unstable, the small planet is removed, but the orbital configuration of the other planets remain unchanged. **B)** Results from previous studies. The stars are representative points from runs starting with 3 equal mass planets on initially coplanar, equally spaced circular orbits with spacings ranging from 0.025 to 1.0 in units of the semi-major axis of the first planet (Duncan 1997). The open circles (two of which are shown as lower limits) are from simulations by Duncan & Lissauer (1998) in which the masses of the four Jovian planets are multiplied by a common scale factor. The filled squares are from studies of the stability of eight inner Uranian moons in which the assumed satellite masses are multiplied by a common scale factor (cf. Duncan & Lissauer 1997).

Fig. 3.— The temporal behavior of Run 12_b, which resulted in a single planet by 3×10^7 years. Each vertical pair of panels shows the orbits of the planets seen face-on (TOP) and edge-on (BOTTOM) at a particular time.

Fig. 4.— Examples of planetary systems generated in our simulations. Positions of a circle along abscissa indicates the planet's semi-major axis. The size of the circle indicates the planetary mass (radius $\propto$ mass$^{1/3}$). In addition, the mass of the planet, in $M_\oplus$, is printed above each planet. The markings beneath each planet indicate the range of distances from the central star (periastron and apastron) with the central vertical line indicating the semi-major axis. A) Our solar system. B) Run 12_b C) Run 6_b D) Run 2_b E) Run 10_b F) Run 14_a G) Run 11_a H) Run 4_a I) Run 5_a J) Run 10_a K) Run 4_b [This system goes through significant macroscopic changes. The double row of marking below each planet indicates the range of distances from the central star at two times: 5.3×10^8 years (top) and 5.6×10^8 years (bottom)]. L) Run 7_b. [This system also goes through significant macroscopic changes. The double row of marking below each planet indicates the range of stellar distance at two times: 1.225×10^9 years (top) and 1.24×10^9 years (bottom).]

Fig. 5.— The temporal behavior of Run 10_b. Each vertical pair of panels shows the orbits of the planets seen face-on (TOP) and edge-on (BOTTOM) at a particular time.

Fig. 6.— The distribution of planets created in our simulations. The green dots refer to planets created in our first set of simulations where the planets had large radii, and thus the system had a significant source of dissipation, for the entire length of the simulations (Series a). The blue circles refer to our set of runs where the planets became small after 10^7 years (Series b). The red stars represent the giant planets in our solar system. The brown stars represents the planets around 16 CygB, 70 Vir, and 47 Uma. A) Mass, M, as a function of semi-major axis, a. B) Eccentricity, e, as a function of mass.

Fig. 7.— A histogram of number of planets in a system. The sum of the gray and black histograms show the results for all of our runs, while the black is for Series a alone.

Fig. 8.— The distribution of our planetary systems: $(L_{TC} - L_T)/L_{TC}$ vs. ζ_{max}. $(L_{TC} - L_T)/L_{TC}$ is a measure of the average eccentricity of the planets in the system, while ζ_{max} is a measure of compactness. The green dots refer to systems created in Series a, and thus systems with a significant source of dissipation for the entire length of the simulations. The blue circles refer to Series b. The blue circles surrounded green show the systems for which are the same in both series. The red '$\odot$' represents the giant planets in the solar system.

Fig. 9.— The variation of the critical argument for the 1:2 mean motion resonance $2\lambda_3 - \lambda_2 - \mu_2$ between the second and third planet in Run 11_a (also see Figure 4G). These planets are very deep in the resonance.

Fig. 10.— The variation of the critical argument for the 1:2 mean motion resonance $2\lambda_3 - \lambda_2 - \mu_2$ between the second and third planets in Run 4_a, see Figure 4H. These planets are weakly trapped in the resonance.

Fig. 11.— The variation of the critical argument for the 7:3 mean motion resonance $7\lambda_2 - 3\lambda_1 - 2\mu_2 - 2\mu_1$ between the first and second planets in Run 5_a (see Figure 4I).

Fig. 12.— The variation of critical arguments of the two resonances found in Run 10_a (see Figure 4J). A) A critical argument of the 5:3 mean motion resonance between the second and third planets, $5\lambda_3 - 3\lambda_2 - 2\Omega_2$. B) A critical argument of the 1:2 mean motion resonance between the third and forth planets.

Fig. 13.— The temporal behavior of the planets resulting from Run 7_b (Figure 4L). Each of the three planets is presented by a different color. A) The periastron distances, q, and aphelion distances, Q, of the planets. The periastron distances and aphelion distances are presented by the solid and dotted curves, respectively. Note that the aphelion curve for the outer planet is off the scale in the figure. B) The inclination of these planets.

Fig. 14.— The orbits of the system from Run 7_b seen at two different times. The left two pan-

els are at 1.225×10^9 years, while the right two are at 1.24×10^9 years. The top panels show the system face-on while the bottom show them edge-on. An animation of this behavior can be found in Appendix A (URL: http://www.boulder.swri.edu/ hal/diversity/appendixA.html).

Table 1. **Parameters for the Initial Embryo Loads**

	β	M_d	B	Number
Load A	2.0	$100M_\oplus$	$\sqrt{3}$	111
Load B	2.5	$100M_\oplus$	$\sqrt{3}$	111
Load C	2.5	$200M_\oplus$	1	180

Table 2. **Input Parameters for the Runs**

	Load	t_g (yr)	t_{neb} (yr)	κ (yr^{-1})
Run 1	A	1×10^5	1×10^6	1.3×10^{-6}
Run 2	A	1×10^6	1×10^6	1.3×10^{-5}
Run 3	A	1×10^7	1×10^6	1.3×10^{-5}
Run 4	A	3×10^5	1×10^6	4.0×10^{-5}
Run 5	A	1×10^6	1×10^6	0
Run 6	A	1×10^9	1×10^6	0
Run 7	A	3×10^5	1×10^6	4.0×10^{-4}
Run 8	A	2×10^5	1×10^6	4.0×10^{-4}
Run 9	A	1×10^5	1×10^7	1.3×10^{-5}
Run 10	B	3×10^5	1×10^6	4.0×10^{-5}
Run 11	B	1×10^5	1×10^6	4.0×10^{-6}
Run 12	B	2×10^5	1×10^6	4.0×10^{-5}
Run 13	B	1×10^6	1×10^6	4.0×10^{-5}
Run 14	B	1×10^7	1×10^6	4.0×10^{-5}
Run 15	C	3×10^5	1×10^6	1.3×10^{-5}
Run 16	C	1×10^6	1×10^6	4.0×10^{-6}

Table 3. **Properties of Stable Systems**

	Series a						Series b					
Run	t_s	N (yrs)	M_{max} ($M_\oplus$)	M_{min} ($M_\oplus$)	M_{tot} ($M_\oplus$)	ζ_{max}	t_s (yrs)	N	M_{max} ($M_\oplus$)	M_{min} ($M_\oplus$)	M_{tot} ($M_\oplus$)	ζ_{max}
1	2.6×10^7	2	1113	592	1305	0.014	1.5×10^8	2	592	509	1102	0.035
2	6.2×10^8	6	26	10	115	0.42	$> 12 \times 10^9$	≤ 3			≤ 38	
3	2.7×10^8	6	27	7	100	0.29	2.6×10^9	2	16	10	26	0.37
4	2.8×10^7	3	85	83	260	0.57	7.9×10^7	3	87	16	190	0.11
5	7.8×10^8	4	54	14	130	0.14	9.8×10^8	2	22	21	45	0.48
6	7.5×10^8	5	30	12	99	0.22	2.7×10^9	2	39	17	57	0.0044
7	9.2×10^7	4	65	13	141	0.16	1.3×10^9	3	42	24	108	0.16
8	7.3×10^6	6	213	8	320	0.46			Same as Series a			
9	1.1×10^7	3	24908	3	24919	0.22	1.1×10^7	2	9974	9	9983	0.015
10	1.8×10^8	5	279	12	553	0.44	3.0×10^8	4	279	3	524	0.18
11	3.5×10^6	5	1261	2	2628	0.41			Same as Series a			
12	1.4×10^8	3	559	15	927	0.18	2.9×10^7	1	343	—	343	—
13	6.7×10^7	4	51	14	124	0.23	5.8×10^8	2	57	28	85	0.0035
14	3.5×10^6	7	26	4	101	0.32			Same as Series a			
15	8.9×10^6	2	868	388	1256	0.091			Same as Series a			
16	5.1×10^8	4	176	20	371	0.12	3.3×10^8	2	140	132	274	0.011

Figure1 —

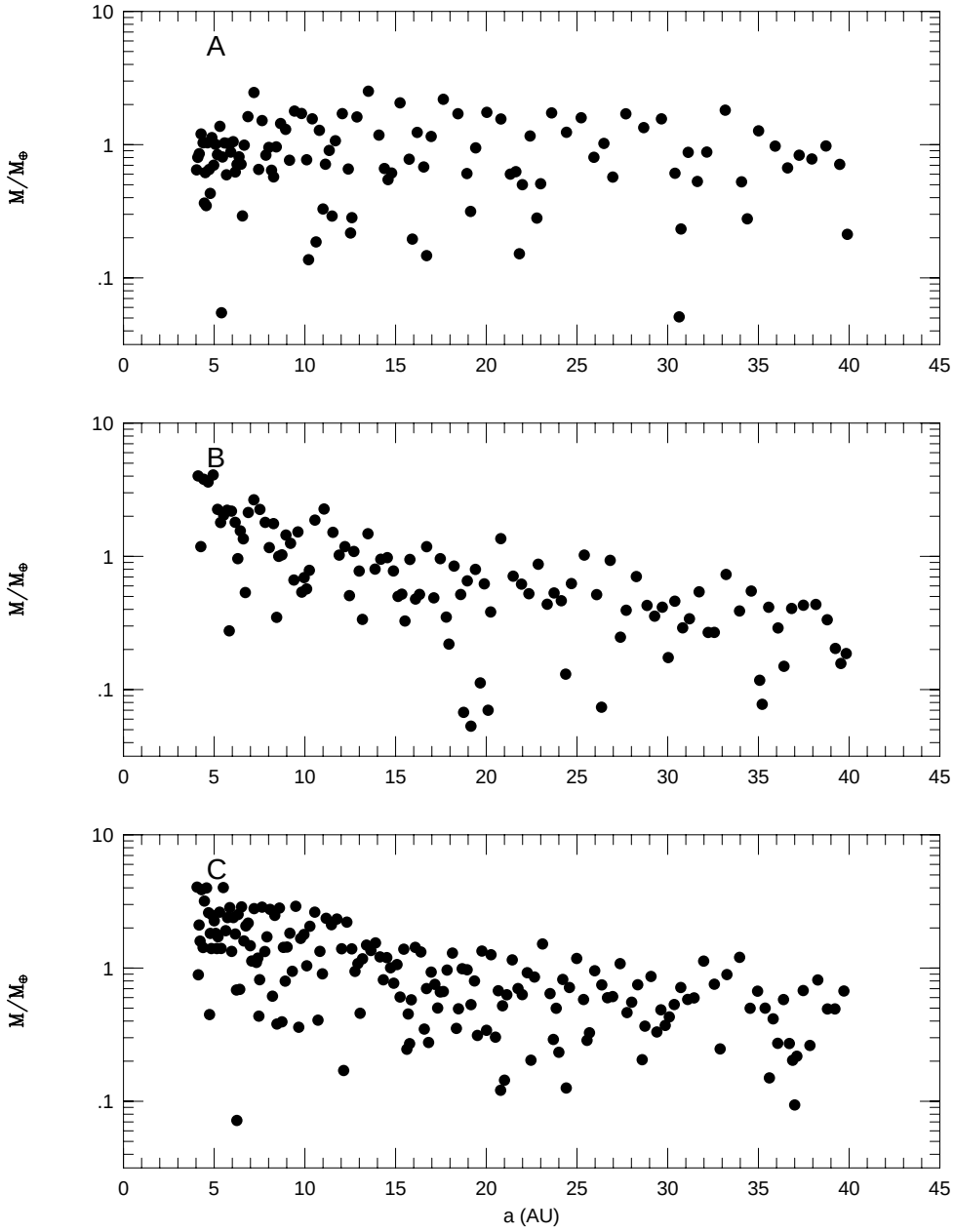

Figure2 —

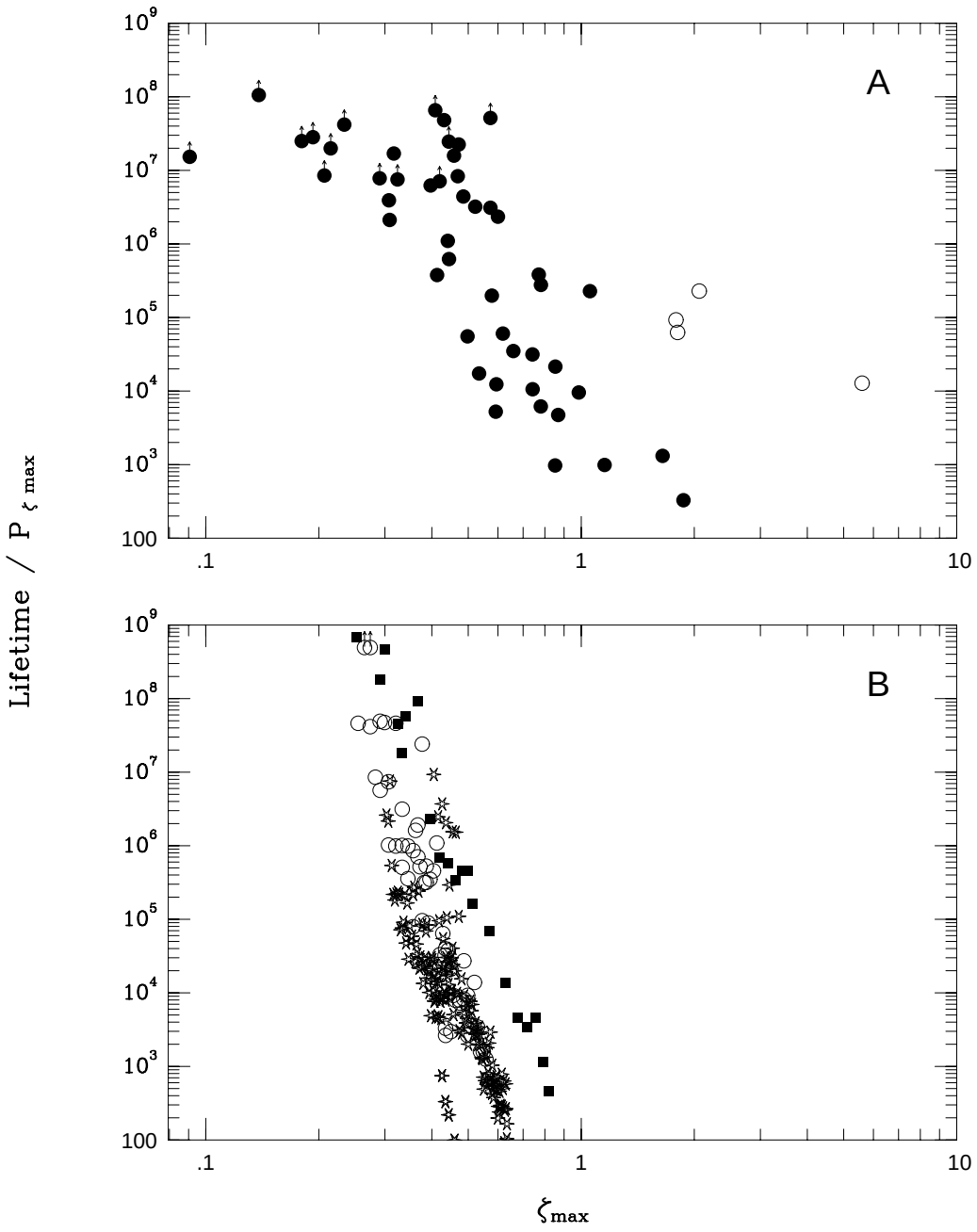

Figure3 —

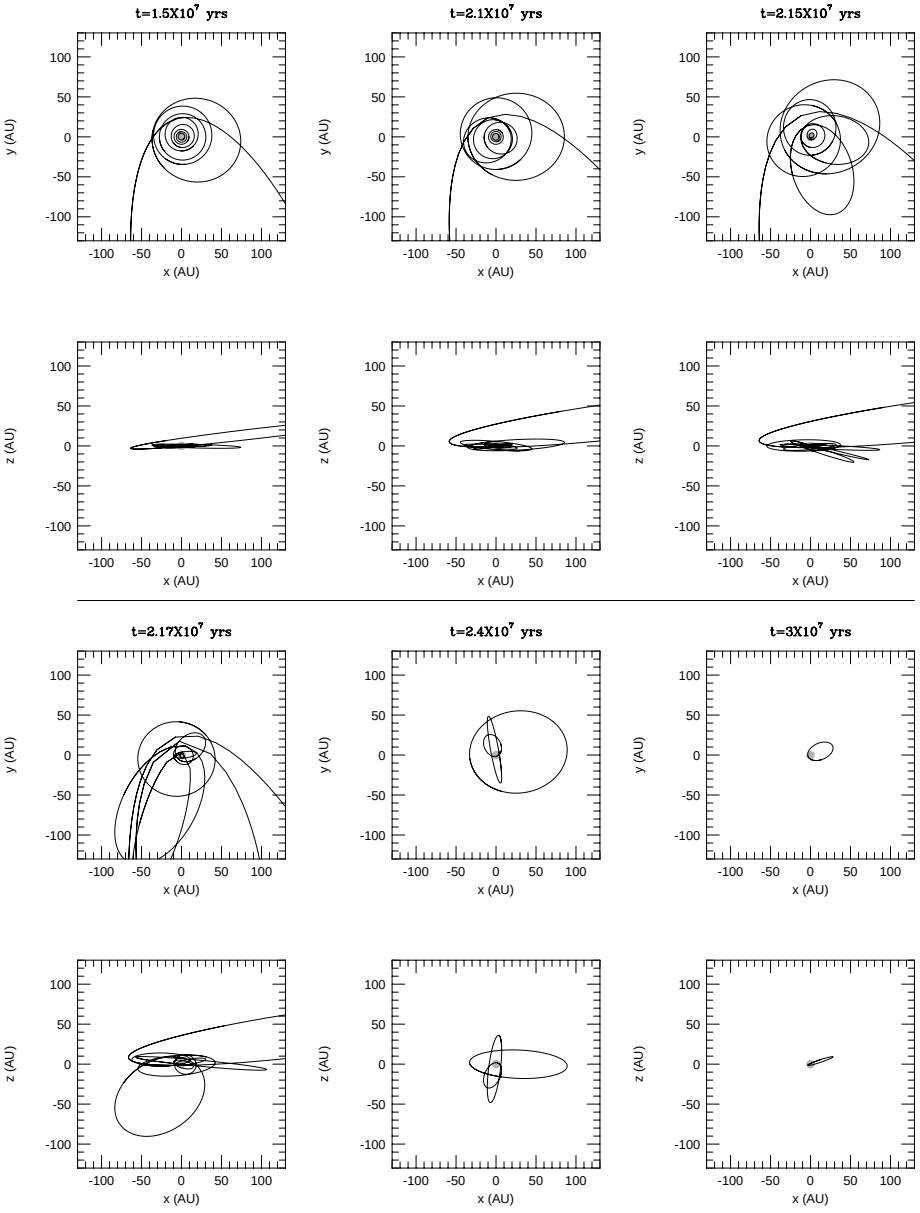
t=1.5X10^7 yrs
t=2.1X10^7 yrs
t=2.15X10^7 yrs
t=2.17X10^7 yrs
t=2.4X10^7 yrs
t=3X10^7 yrs
y (AU)
z (AU)
x (AU)
100
50
0
-50
-100

Figure4 —

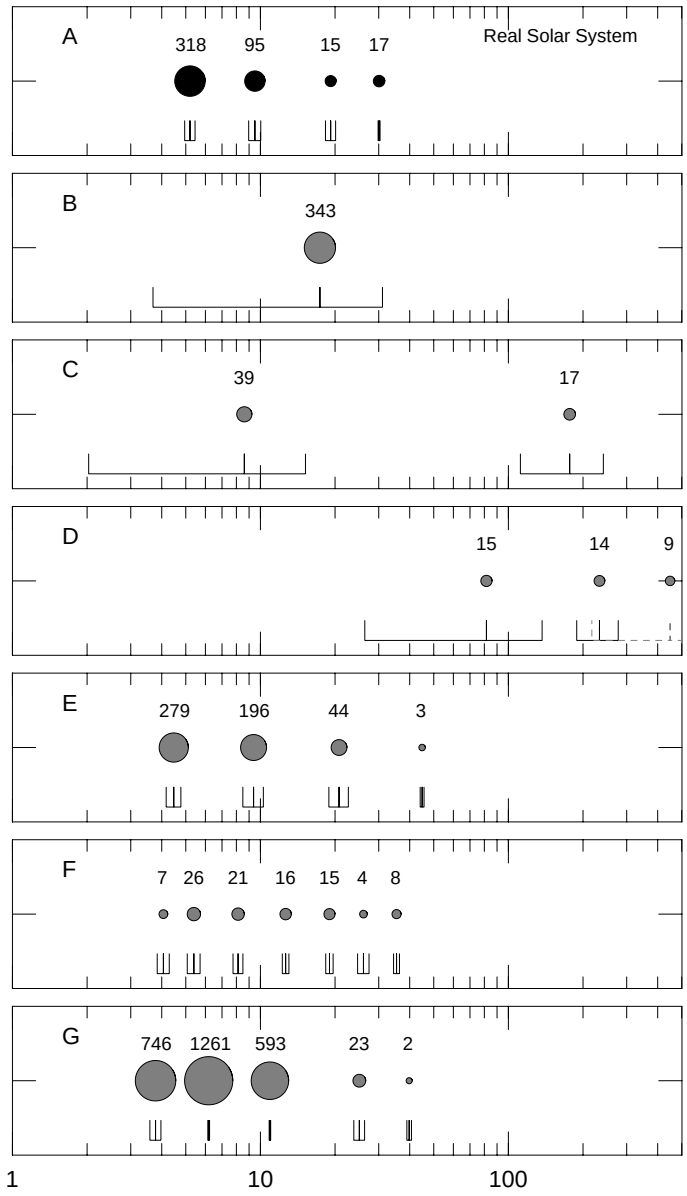
A
318
95
15
17
Real Solar System
B
343
C
39
17
D
15
14
9
E
279
196
44
3
F
7
26
21
16
15
4
8
G
746
1261
593
23
2
1
10
100

Figure4 (cont.) —

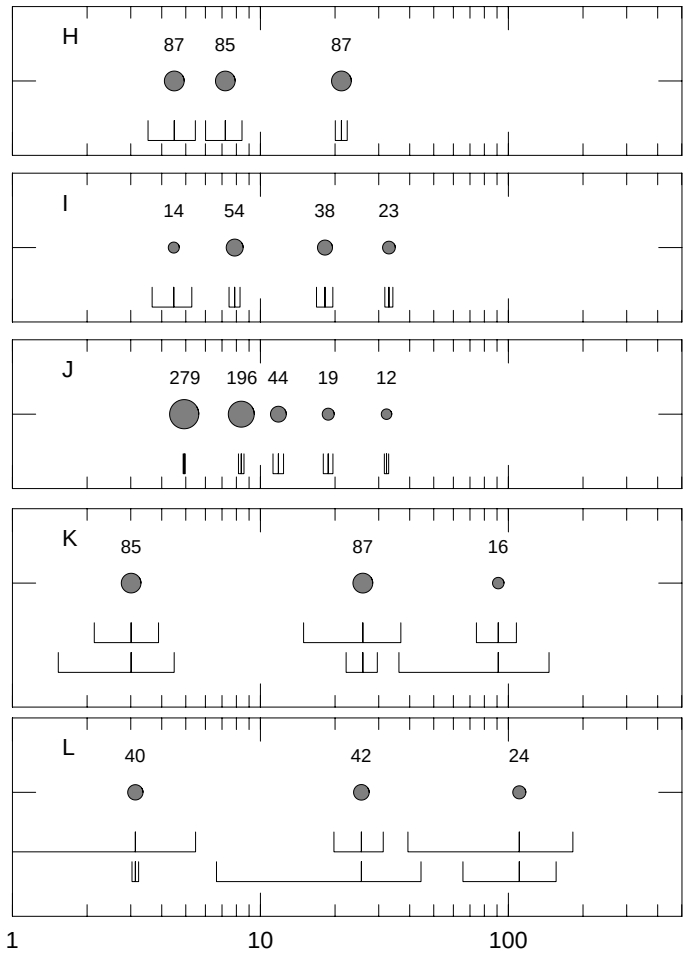

Figure5 —

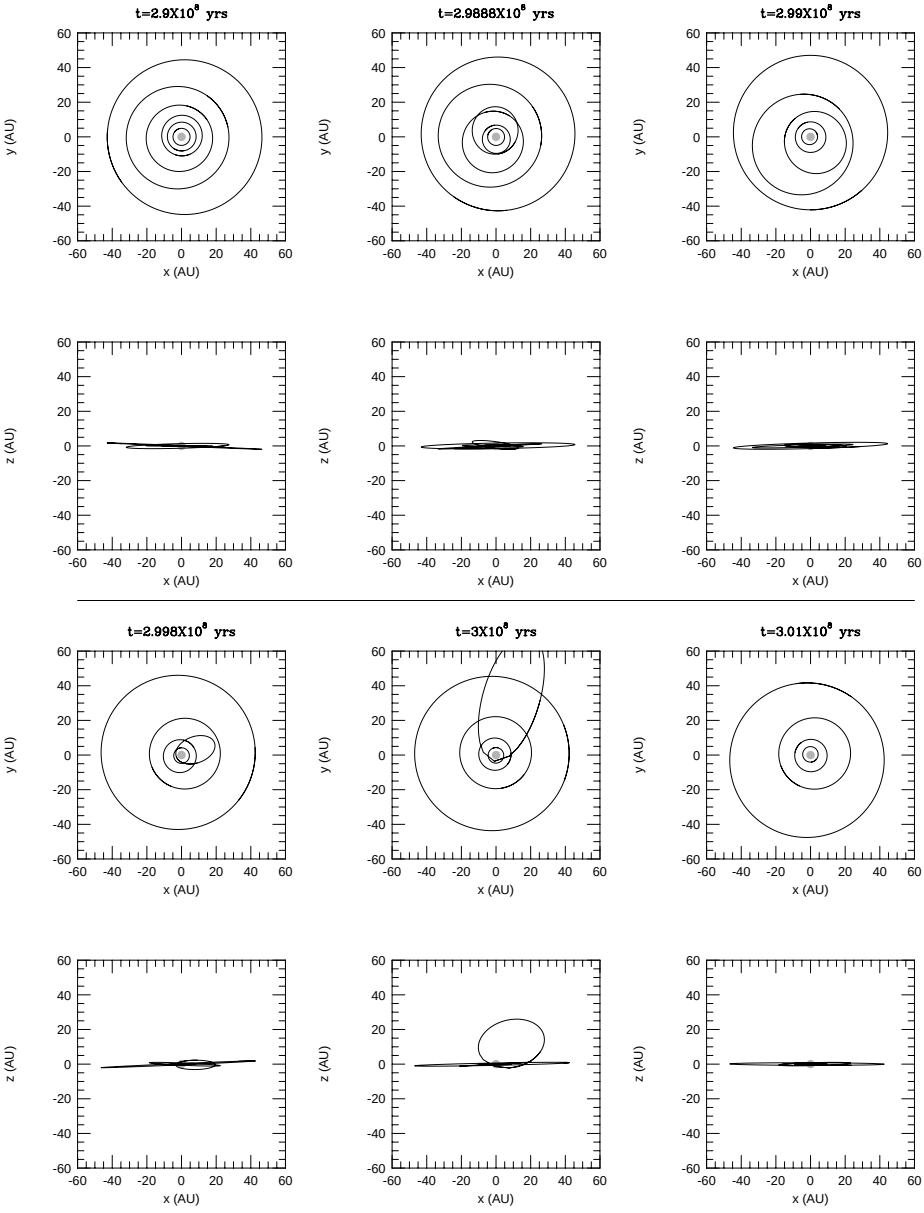
t=2.9X10^8 yrs
t=2.9888X10^8 yrs
t=2.99X10^8 yrs
t=2.998X10^8 yrs
t=3X10^8 yrs
t=3.01X10^8 yrs
y (AU)
z (AU)
x (AU)

Figure6 —

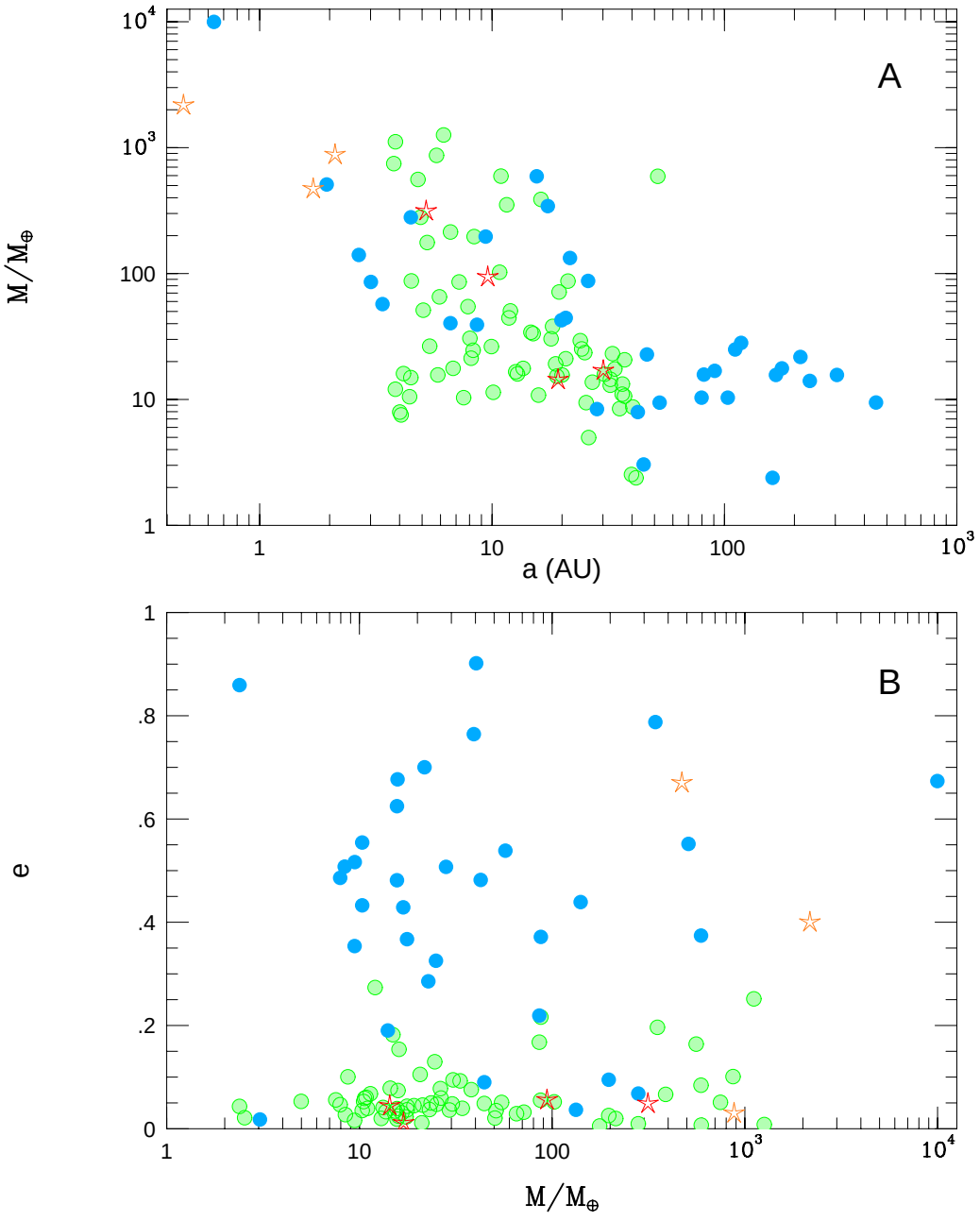

Figure7 —

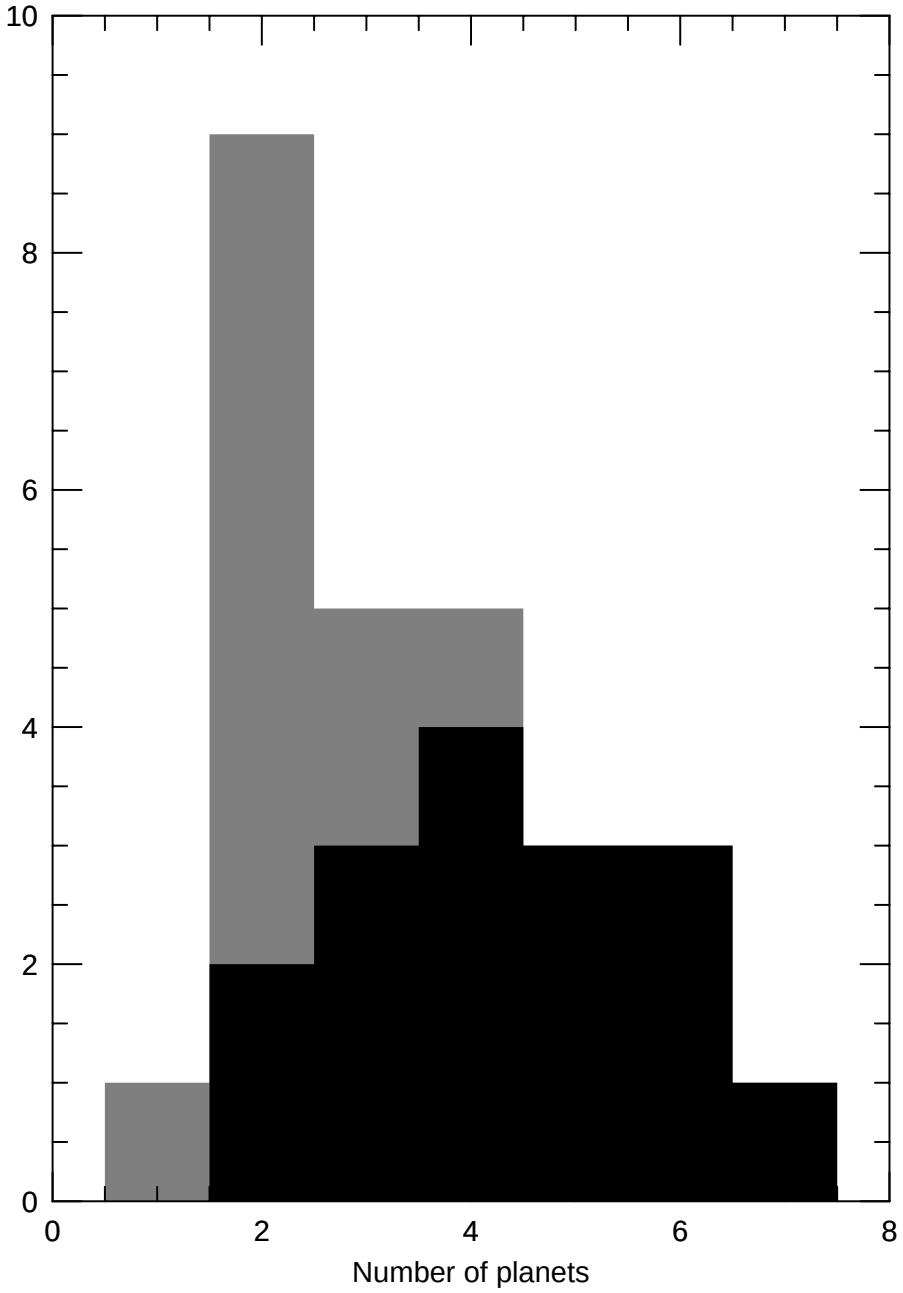

Figure8 —

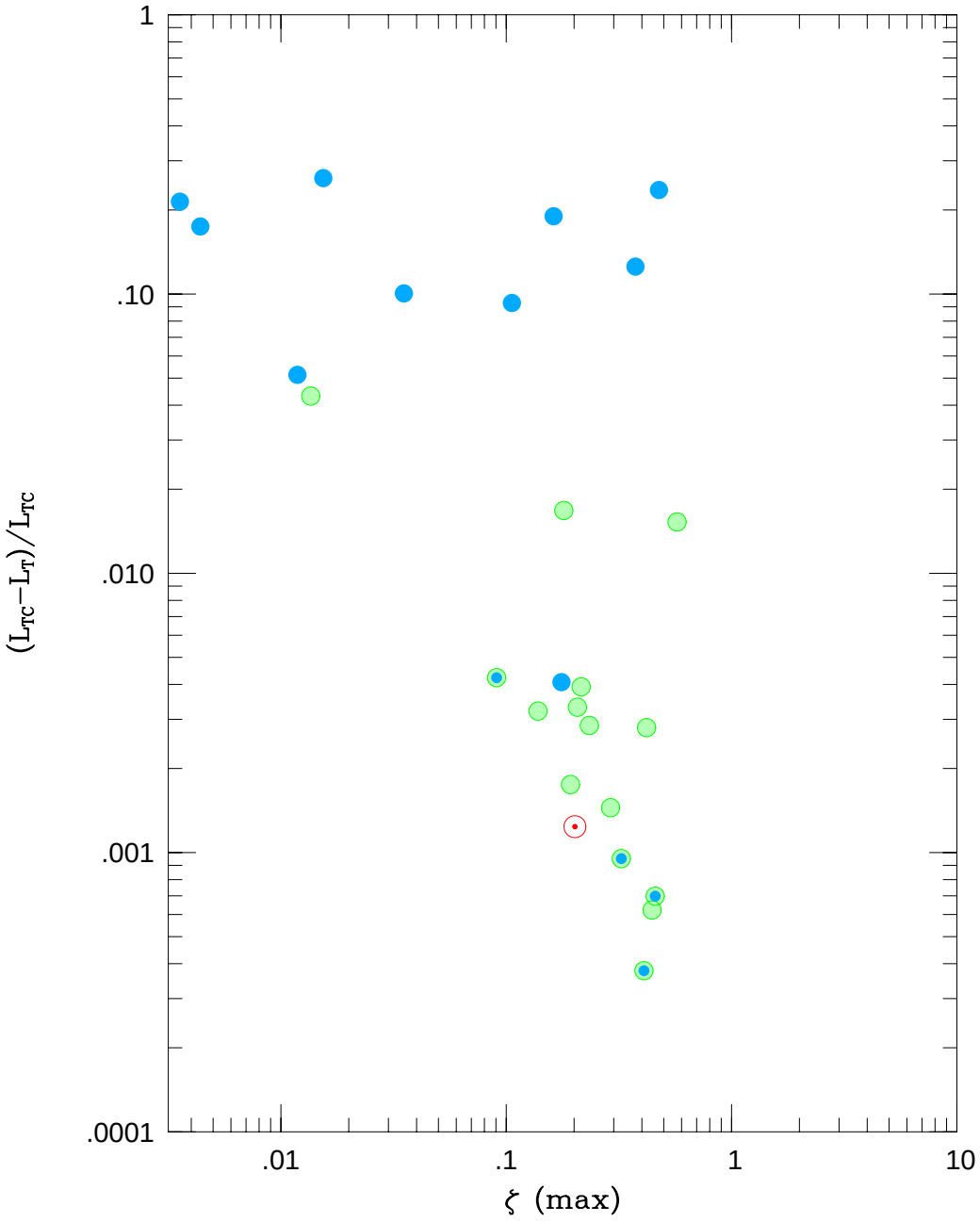

Figure9 —

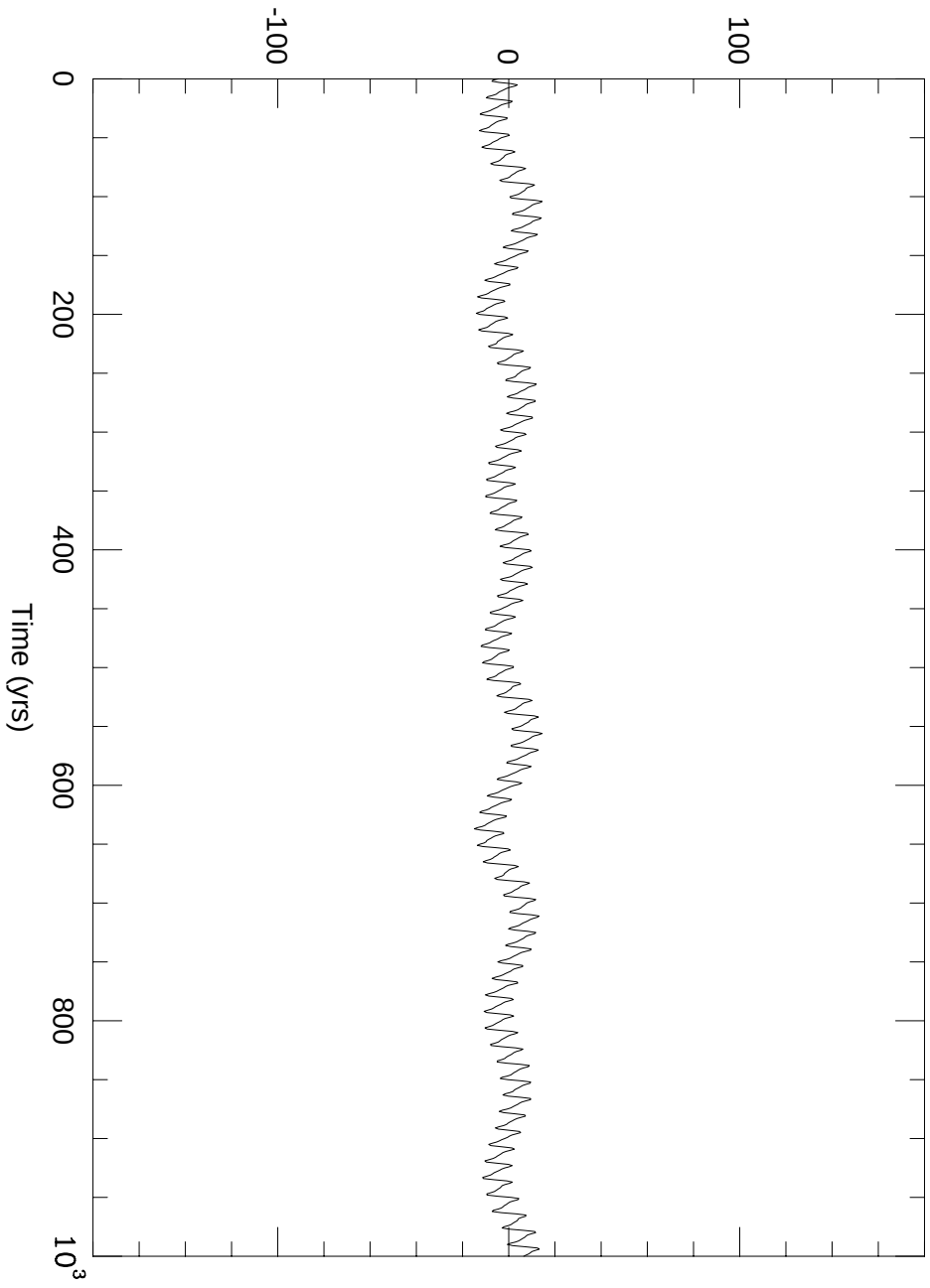

Figure10 —

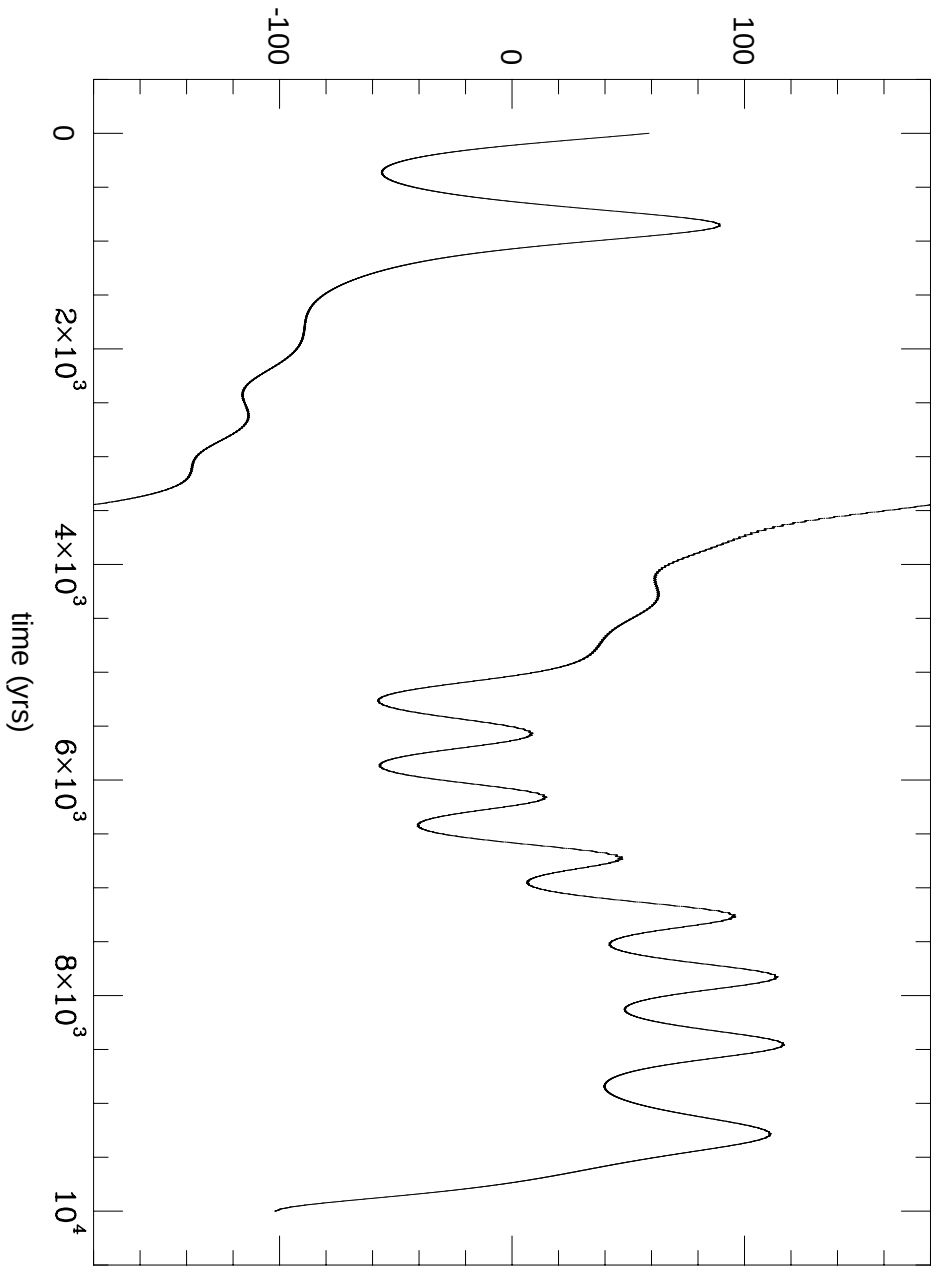
$2\lambda_2-\lambda_1-\mu_1$
-100
0
100
0
2×10^3
4×10^3
6×10^3
8×10^3
10^4
time (yrs)

Figure11 —

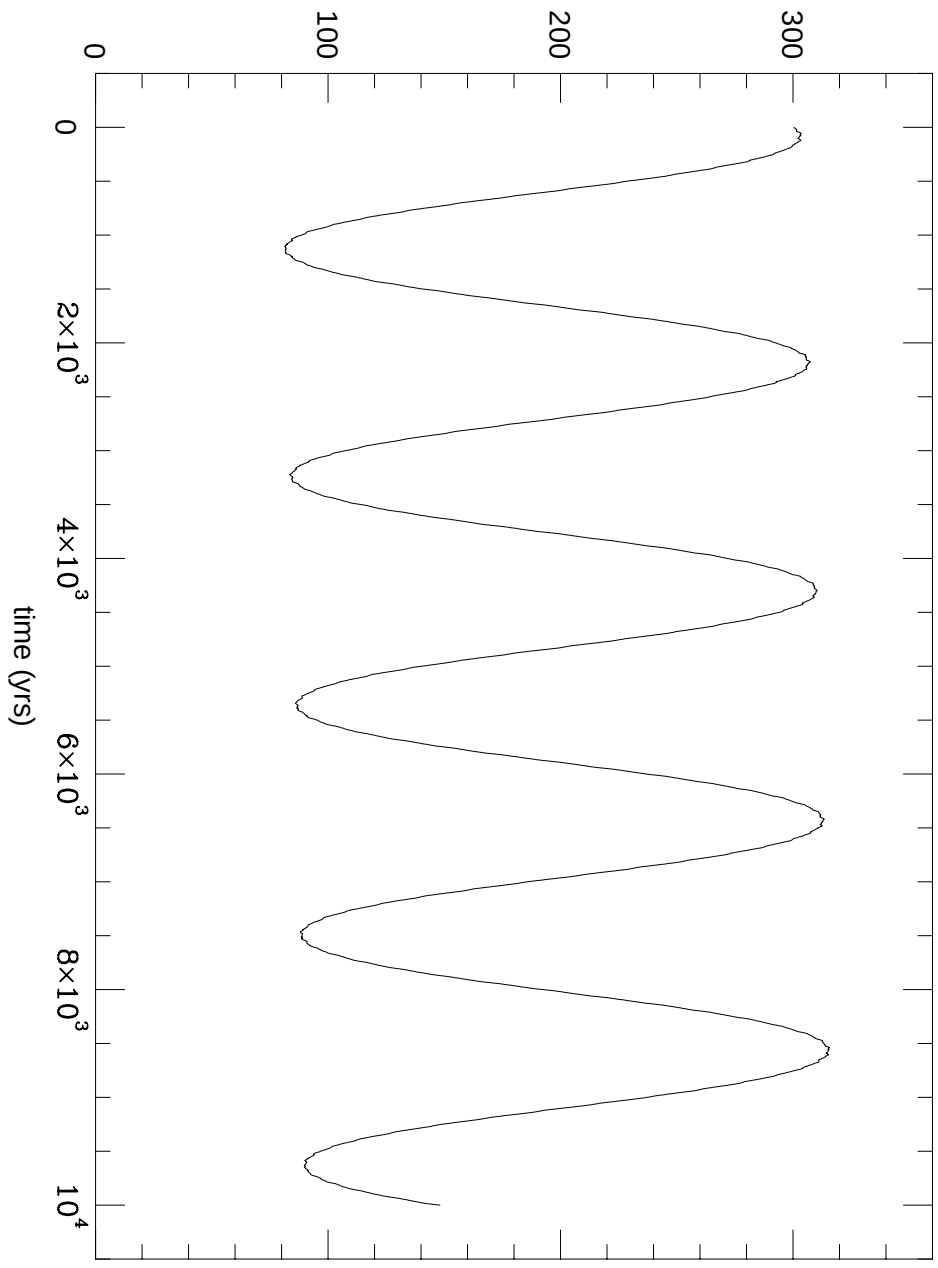
$7\lambda_2-3\lambda_1-2\mu_2-2\mu_1$
0
100
200
300
0
2×10^3
4×10^3
6×10^3
8×10^3
10^4
time (yrs)

Figure12 —

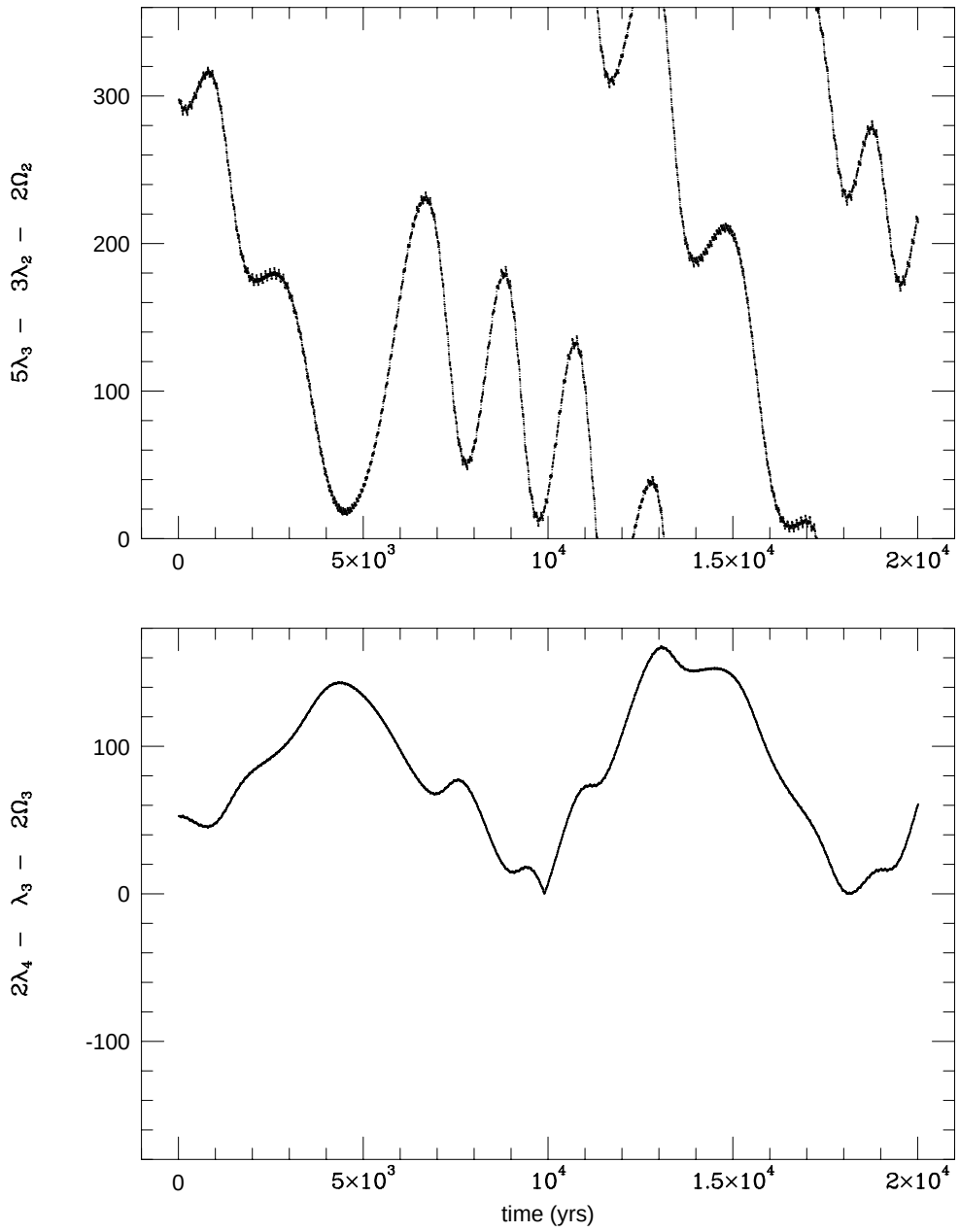
$5\lambda_3 - 3\lambda_2 - 2\Omega_2$
300
200
100
0
0
5×10^3
10^4
1.5×10^4
2×10^4
$2\lambda_4 - \lambda_3 - 2\Omega_3$
100
0
-100
0
5×10^3
10^4
1.5×10^4
2×10^4
time (yrs)

Figure13 —

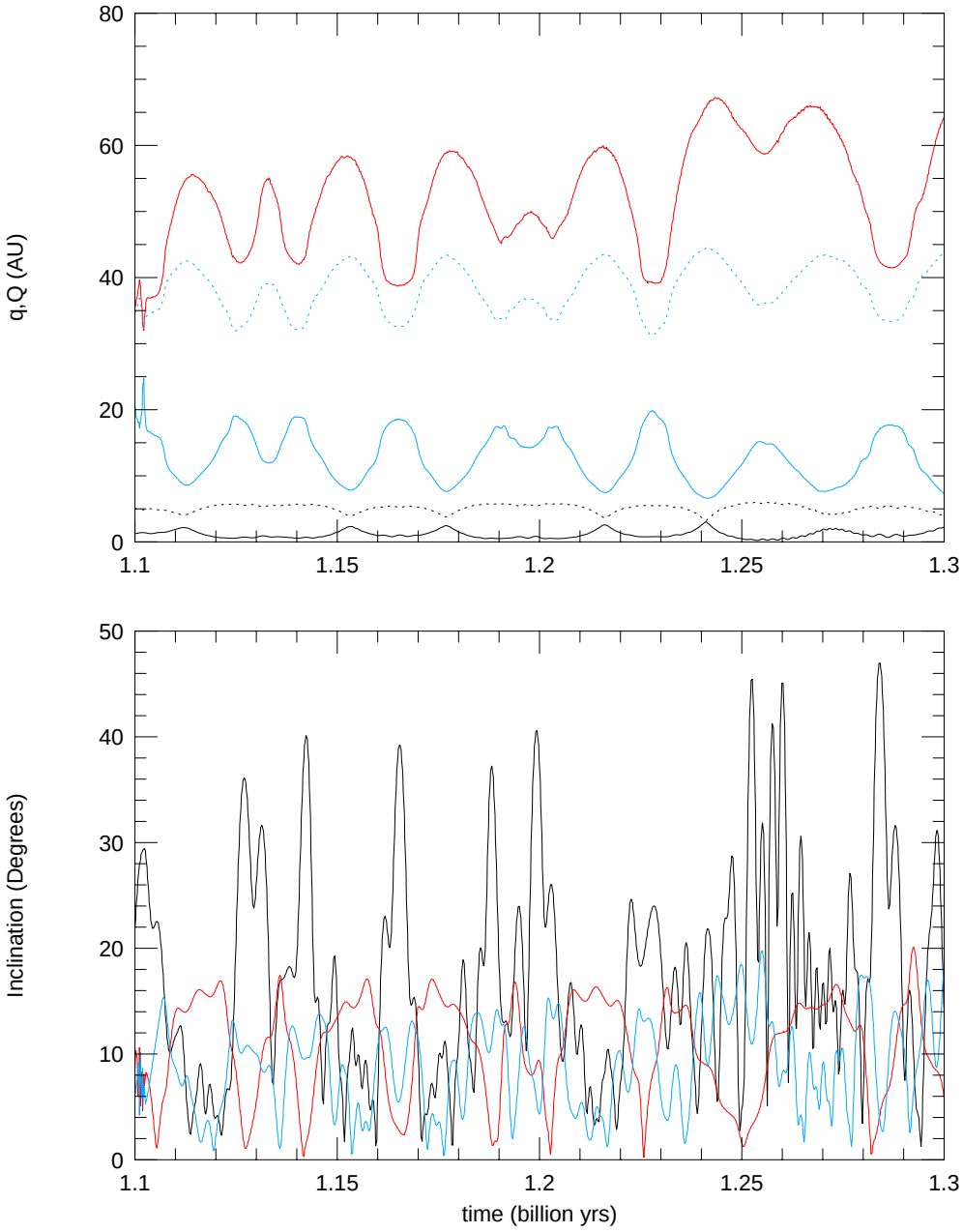
80
60
40
20
0
q,Q (AU)
1.1
1.15
1.2
1.25
1.3
50
40
30
20
10
0
Inclination (Degrees)
1.1
1.15
1.2
1.25
1.3
time (billion yrs)

Figure14 —